Rosa

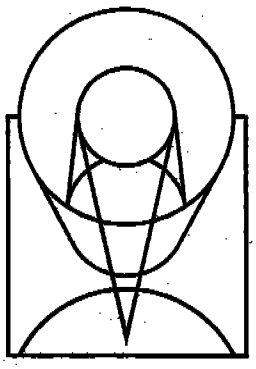

SPACE TELESCOPE SCIENCE INSTITUTE

INSTRUMENT SCIENCE REPORT
CAL/FOS-016

THE LABORATORY ABSOLUTE PHOTOMETRIC CALIBRATION OF THE FOS

G. F. Hartig

R. C. Bohlin

June 1985

SPACE TELESCOPE SCIENCE INSTITUTE
Homewood Campus Baltimore, MD 21218

Operated by the Association of Universities for Research in Astronomy, Inc., for the National Aeronautics and Space Administration

INSTRUMENT SCIENCE REPORT

CAL/FOS-016

THE LABORATORY ABSOLUTE PHOTOMETRIC CALIBRATION OF THE FOS

George Hartig and Ralph Bohlin

June 1985

Abstract

A synopsis of the laboratory measurements of the FOS absolute spectrophotometric efficiency in most of its optical configurations is presented. These measurements are compared with those predicted on the basis of earlier evaluations of the efficiencies of the individual components: mirrors, dispersers and filters, and the Digicon quantum efficiencies. Some evidence for minor degradation in performance is present; however, discrepancies between the predicted and measured throughput are generally within the estimated error. Final estimates of the current FOS throughput for each disperser are tabulated.

CONTENTS

1. Introduction

This report presents a detailed summary of the relevant measurements which have been made to date in order to estimate the absolute photometric efficiency of the FOS in its standard high and low resolution spectrophotometric modes. The FOS efficiency for spectropolarimetry will be discussed elsewhere. The determination of the FOS quantum throughput efficiency (QT) is an indirect process involving several sequential calibrations, each with associated measurement error resulting from statistical fluctuations as well as systematic effects. While estimates of the statistical uncertainties can be made with confidence, the degree to which systematic effects degrade the calibration accuracy is generally difficult to estimate. Where possible, several independent measurements of the QT have been made in order to increase the confidence level and to provide indications of the extent to which systematic errors affect the results.

The QT has been determined in two separate ways: 'end-to-end' calibration against previously calibrated standard light sources and from multiplication of the individually measured efficiencies of the optical components and the detector quantum efficiencies (QE). The former method involved the design, construction and absolute calibration of two devices called the Ambient and the Vacuum Space Telescope Optical Simulators (ASTOS and VSTOS). These provide a means of illuminating the FOS in a manner similar to that of the ST, with continuum and spectral line light sources covering the entire wavelength range over which it is sensitive (~λλ1200-8500Å). The ASTOS and VSTOS and their absolute calibrations at the NBS are discussed in the next section, and their applications to determine FOS QTs are described in

section 3. The individual component measurements are briefly described in section 4. An analysis and intercomparison of the calibration data are presented, followed by our final estimate of the actual FOS QT for each spectrophotometric mode in section 5.

2. The Space Telescope Optical Simulators (STOSs)

Two separate devices were designed and constructed by Martin Marietta-Denver Aerospace (MMDA) specifically for the FOS throughput measurements: the ambient STOS (ASTOS), for use in air at wavelengths above λ2000Å, and the vacuum STOS (VTOS) for the far ultraviolet (FUV). Each was calibrated at the NBS (at separate facilities) both before and after the FOS calibration to assure that significant changes did not occur in their spectral irradiance at the FOS entrance aperture plane, or at least to permit an estimate of the uncertainties in the FOS measurements due to such fluctuations. Description of each of these devices, their calibration methods and uncertainties in the irradiance determinations are discussed separately for each STOS in the following sections.

2.1 The ASTOS

The ASTOS is the simpler of the two simulators, consisting basically of a means of supporting a light source in front of a barium sulfate-coated diffusing screen. A circular aperture with a central occulting disk is positioned so as to limit the solid angle of diffusing screen seen by the FOS

to an f/24 beam with 14% obscuration, mimicking the ST Optical Telescope Assembly (OTA). A 1000W tungsten 'FEL' lamp and a Gamma Scientific deuterium lamp provide combined coverage of the spectral region from λ2000 to λ8500Å. A more detailed description of the ASTOS may be found in Appendix A of the FOS Calibration Report (Harms, et al. 1985), hereafter referred to as the Calibration Report.

2.2 ASTOS Calibration

2.2.1 Method

The ASTOS was calibrated in December 1982 and September 1984 at the FASCAL facility at the NBS in Gaithersburg, MD, by Mr. James Walker under the auspices of Mr. Donald McSparron. The same methods were employed for both calibrations although some improvements in automatic data acquisition capability were made in the interim. The calibrations were performed in two parts: above λ3000, the ASTOS spectral irradiance (or 'monochromatic flux', in units such as erg $s^{-1}cm^{-1}Å^{-1}$, or Wcm^{-3}) with each of two FEL lamps installed was measured directly by comparison with a 'shelf standard' FEL lamp whose irradiance had been previously calibrated against a black body source. The ASTOS irradiance was too weak below λ3000 for accurate measurement in this configuration, which employs an integrating sphere in front of the NBS monochromator entrance slit. For shorter wavelengths (including all of the D_2 lamp measurements), the ASTOS radiance (or 'specific intensity', in units such as erg $s^{-1}cm^{-2}Å^{-1}arcsec^{-2}$, or W $cm^{-3}sr^{-1}$) was measured and the irradiance calculated from the geometry. The irradiance calculated in this way was found

to agree to within ~2% with the directly measured irradiance at λ4000. The same special power supply was used, without adjustment, for each of the D_2 lamp measurements, so the lamp operating current was presumably constant throughout the calibration period. The FEL lamps were operated nominally at 8.000 amps, but because of several failures of the Optronics power supply requiring the use of alternate supplies and the use of several different shunts and voltmeters to determine the lamp current, there exists an uncertainty of about 10 mA in the operating current during various phases of the calibration. The Sept. 84 NBS calibrations were performed at 8.010 amps, since this is the current produced by the supply at the 8.011 dial setting used for the FOS calibrations (as measured by the NBS), and is most probably representative of the actual lamp current during the August FOS absolute photometric calibration (APC) measurements. The difference in irradiance between 8.000 and 8.010 amps amounts to at most 2% at the shortest wavelengths used and is typically <1%, a small fraction of the estimated uncertainty in the ASTOS calibration. Details of the measurements and the techniques whereby the ASTOS was aligned with the monochromator are given in the NBS Report of Calibration, in Appendix A of the Calibration Report.

2.2.2 NBS Results

The measured ASTOS irradiances are also included in Appendix A of the Calibration Report. A formal report for the latest (Sept. 84) calibration has not yet been received from the NBS; however, the data has been reduced and is included in the Appendix. The results of interest are those for the FEL lamps GS179 and GS180, and D_2 lamp DL116, each with diffuser #2, since these are the

components used for actual FOS absolute photometric calibration APC measurements. The agreement between the 1982 and 1984 FEL lamp calibrations is excellent. Discrepancies are typically less than 2% for GS179 and 4% for GS180, and are well within the uncertainties stated by the NBS, which range between 5 and 8%. This agreement extends over the entire wavelength range from λ2500 to λ8500Å.

The agreement for the D_2 lamps is not nearly so good, particularly at short wavelengths. An investigation into the cause of the discrepancies led to the discovery of an error in the technique used to calibrate the NBS secondary radiance standard at short wavelengths, involving incorrect dark current subtraction and the realization that at λ2000 approximately 95% of the signal is due to scattered light. The former difficulty was corrected with a careful recalibration of the standard, but the scattered light problem inflated the estimated uncertainty at λ2000 to a factor of 3, at λ2100 to ±30%, and at λ2500 to ±8%. These large uncertainties still do not account for all of the discrepancy between 1982 and 1984 calibrations and we suspect that the lamp may suffer variations in intensity and/or spectral distribution (see section 3.2).

2.3 The VSTOS

2.3.1 Design

The vacuum STOS is a more intricate device than the ASTOS, since it must be capable of repeatably positioning a number of light sources (the FUV sources tend to cover a fairly limited wavelength range) in such a manner as

to properly simulate the illumination from ST. This is accomplished by a motorized carousel, which carries the following lamps: two Pt-Cr/Ne hollow cathode lamps (of the same type used on board the FOS for wavelength calibration, but with flat MgF_2 windows in place of the lenses used on the FOS flight lamps), a Quantatec krypton dimer lamp, a Quantatec hydrogen lamp, and a Resonance, Ltd. argon dimer lamp. The latter three provide smooth continuum spectral distributions while the hollow cathode lamps, one of which has a MgF_2 diffuser (8μ surface roughness on one side) installed over its window, provide spectral lines which span the entire wavelength range of interest. The source volume of the selected lamp is imaged onto the FOS entrance apertures with an f/24 beam by a small, inverted Cassegrain telescope, with MgF_2/Al coated mirrors and central obscuration ratio matching ST. A motorized polarizer which can efficiently plane-polarize the beam at a range of angles in 22.5 degree steps is also included. The carousel and polarizer are actuated by means of a special control box. A more detailed description of the VSTOS may be found in Appendix B of the Calibration Report.

2.3.2 VSTOS Performance

Because of the focussed nature of the VSTOS beam and the fairly small size of the lamp images it is inherently susceptible to producing variations in the flux seen by the FOS as a result of carousel non-repeatability, misalignment with the FOS and lamp source volume migration. These possible sources of error in the FOS APC are exacerbated by the nonuniform, sometimes highly asymmetrical spatial flux distribution of the VSTOS images; furthermore, this distribution was found to have strong wavelength dependence for

some lamps. Not surprisingly, the flux levels were also found to vary, especially for the continuum lamps, and the degree of variability is also dependent on wavelength. Some evidence exists that the rate of variation may be dependent on the lamp use duty-cycle. Some of these difficulties were not apparent at the outset, but were discovered while the APC was in progress. Nevertheless, we believe that a useful calibration of the FOS blue side UV efficiency has been obtained with the VSTOS by careful alignments and judicious choice of data, based on measurements and estimates of the degree to which these deleterious effects operate.

2.3.2.1 Carousel Repeatability

For the reasons stated above, the VSTOS lamp carousel must be capable of positioning the lamps very accurately and repeatably on the axis of the imaging optics. Tests have shown that the carousel is quite repeatable if undisturbed and if the multiple lamp power cables, which must be free to rotate with the carousel, are carefully draped, so as not to bind or cause excessive torque. This has been possible in practice throughout the calibrations procedures, although some difficulty was encountered with proper actuation of the reset fiducial switch. Small changes in wheel balance and cable-induced torque could change the stepper motor phase at which this switch was actuated, causing each lamp to be positioned one motor step off axis thereafter. Since one motor step moves the lamp image by a significant fraction of its width, a means of mitigating this sensitivity had to be devised. This took the form of an LED on the control panel to indicate when the correct motor phase had been achieved at reset (added during the May 84

NBS calibration) and the addition of single step control of the carousel (installed at MMDA prior to the FOS vacuum calibration in July '84: T/V 3). The carousel is also susceptible to a misphasing, if it is manually rotated by one or more turns from the orientation in which it was aligned. This is because the gear ratio between stepper motor pinion and carousel gear does not provide an integral number of motor steps per carousel revolution. Care was generally taken in this regard, but evidence exists that such a misphasing occurred when the VSTOS was mounted and aligned with the FOS just prior to T/V 3. Single step mapping of the lamp images with the FOS showed that the image centers were approximately one step off of the nominal position. Calibration data were subsequently obtained by single-stepping each lamp to its approximate image center.

2.3.2.2 Spatial Distribution of Lamp Flux

The image of each of the five VSTOS lamps was carefully mapped with a silicon detector when the lamps were initially aligned prior to the first NBS calibration (Hartig, 1984). The detector window was coated with sodium salicylate to enhance its UV response. In general, the light distribution in the images was found to be fairly symmetrical and broad enough that reasonable care in alignment would yield a satisfactory calibration. After the addition of the carousel single-step capability we were able to map the images in the FUV (during T/V 3). These data demonstrated that, especially for the argon lamp, the FUV flux distribution is markedly different from that in the visible and near UV, indicating that these emissions are produced in different regions of the lamp. The argon FUV image was found to be grossly asymmetric and

displaced from the center of the image at longer wavelengths. The Kr lamp also exhibited an FUV flux distribution different from that in the visible. More detailed UV mapping in both vertical and horizontal axes was performed during the NBS recalibration of the VSTOS; the results are shown in Figure 2.1. The hollow cathode Pt-Cr/Ne lamps have no obvious wavelength dependence in this regard (as expected) and the diffused lamp has a very broad distribution, making it particularly insensitive to alignment errors.

2.4 VSTOS Calibration

The VSTOS was calibrated at the NBS by a team consisting primarily of Drs. Jules Z. Klose (NBS), Merv Bridges (NBS), the author, and Mr. Elden Constable and Mr. William Miles (MMDA). The consultation services of Dr. Henry Kostkowski were also employed. Separate calibrations were performed in late May and early August 1984, bracketing the FOS T/V 3 APC.

2.4.1 The NBS Vacuum Calibration System

The apparatus used for VSTOS calibration consists of a one meter Seya-Namioka vacuum UV monochromator with 1200 gr/mm concave grating, an EMR 541F-09-18 CsTe cathode photomultiplier tube (operated at 1900V), a picoammeter and chart recorder. This was used to compare the spectral irradiances of the VSTOS with argon arc sources of known irradiance in the wavelength range from λ1200 to λ3000Å. There exists a fundamental mismatch between these sources however: the VSTOS produces an f/24 beam with 14% central obscuration, while the argon arc sources provide much more collimated beams. Furthermore, the

monochromator grating was found to be masked such that it would not accept the full VSTOS beam. A new mask was made to alleviate this problem but it was later discovered that the high degree of astigmatism of the Seya mounting, combined with the small (~9.5 mm diameter) active area of the PMT photocathode, effectively limited the beam to about f/30. A careful mapping of the relative response of the monochromator at a variety of wavelengths was thus required in order to properly compensate for the partial beam loss and nonuniformities in grating and photocathode efficiency. We note that this method represents a departure from the standard method for irradiance calibration, in which a diffuser is placed behind the monochromator entrance aperture to avoid beam mismatch problems; however, the VSTOS flux levels, especially at short wavelengths, precluded this approach and necessitated the mapping.

2.4.2 Calibration of the NBS Monochromator

The NBS monochromator was calibrated (PMT current out vs. spectral irradiance incident on its entrance aperture) in June-July 1984, following the May 84 VSTOS measurements and again in August, immediately following the VSTOS re-calibrations. Measurements were made with both .5 and 1mm circular entrance apertures, with .8 and 1.8mm exit slit widths, respectively, matching the configuration used for the VSTOS. The 1mm aperture remained fixed to the entrance slits of the monochromator throughout the May-August calibration

period to eliminate possible errors (due to system nonuniformities) that might arise if its registration were altered. The 1/2mm aperture when required, was registered as well as possible, with the aid of a needle, with the center of the 1mm aperture.

2.4.2.1 Method

The calibration was performed, from λ2000 to λ3100Å, with an argon mini-arc, designated 'NBS-5', which had been previously calibrated as an irradiance standard (in March 1983) against an argon maxi-arc radiance standard following the method described by Ott, Bridges and Klose (1980). Briefly, the known relative spectral flux distribution of the radiance source is used to calibrate, on a relative scale, the irradiance of the mini-arc. This is put on an absolute scale by comparison with a tungsten halogen 'FEL' lamp (designated 'F-66') calibrated irradiance source, at the longer wavelengths, since the geometric factors involved should be independent of wavelength. The mini-arc was not calibrated below λ2000 and since the maxi-arc has substantially greater flux (required for accurate calibration at the shortest wavelengths), 'MAXI I' was used for calibration below λ2000. The same method was employed, i.e. its known spectral radiance was converted to irradiance at the monochromator entrance slit by comparison with the NBS-5 mini-arc in the region of overlap (above λ2000). The original maxi-arc radiance calibration was performed by comparison with a hydrogen arc whose radiance is calculable (Ott, Behringer and Gieres 1975 and Ott, Fieffe-Prevost and Wiese 1973).

In each case, the MgF_2 window used to isolate the VSTOS vacuum chamber (and therefore in the VSTOS beam during its measurements) was placed between the arc and the entrance aperture. A cursory mapping of this window, made by moving it around in the (narrow) maxi-arc beam, indicated that its transmittance was quite uniform, so beam size and window position considerations are insignificant. The volume between this window and the monochromator entrance port assembly window (also MgF_2) was flushed with argon during all calibration measurements, and care was taken to assure that no volume of trapped air was present in the lamp/window configurations. (This was a problem in our first attempts to perform the calibration).

2.4.2.2 Mapping

Because of the mismatch between the narrow arc beam and the f/24 VSTOS beam, the response of the monochromator at various incidence angles (relative to that on-axis) had to be mapped out. This was accomplished by mounting the maxi-arc on a special fixture so that it could be rotated horizontally about a point directly beneath the entrance aperture, while jack screws could be turned to do the same in the vertical direction. Mapping was performed over the approximately ±1.2 degree angles of incidence that define an f/24 beam. Fairly strong wavelength dependence was found, so the mapping was undertaken at 10 wavelengths covering the λλ1200-3000 range. Relatively small variations occurred as the beam was moved horizontally, but strong dependence on vertical angle was evident. This is interpreted as evidence that the grating efficiency is fairly uniform but the PMT photocathode response varies markedly as the image is moved up and down along the monochromator exit slit. Mapping was

performed only along the axes (which intersect at the monochromator optical axis), the efficiency at other points in the beam was assumed to be sufficiently well represented by the product of the efficiencies at corresponding points on the axes. Then, assuming a perfectly uniform distribution of flux in the VSTOS beam, the monochromator response to its f/24, centrally obscured beam was calculated relative to the maxi-arc beam on-axis. This result, shown in Figure 2.2, was then applied to the monochromator calibration to estimate its true response to the VSTOS beam.

2.4.2.3 Calibration Uncertainties

The signal levels involved for all of the argon arc calibrations are high enough that system noise is essentially negligible and statistical uncertainties are dominated by our ability to read the chart recordings; typical accuracy is ±2%. The NBS-quoted uncertainty in the absolute radiance calibration of the MAXI-I arc ranges from ±5% above λ1500, degrading to ±10% at shorter wavelengths, where the continuum is contaminated by variable emission lines. The absolute irradiance of the NBS-5 mini-arc is known to within 6% over the interval λλ2000-3200; independent measurements of the arc irradiance in August 1982 and March 1983 agree to within ±2%. Systematic errors in the monochromator calibration may also be important but are difficult to estimate. Some possible source of such error are:

1. Misalignment of the arc with the monochromator axis. The mapping of the response allows us to make an estimate of the error due to angular misalignment; estimating that maximum possible such alignment error is

less than ±.1°, the uncertainty is ±4%. The arc source beams are narrow and nearly collimated so they must be well centered on the entrance aperture; however, care was taken to maximize the signal, so this source of error becomes minimal.

2. Non-linearity of the PMT, picoammeter or chart recorder. The latter two instruments have been calibrated and we expect error contributions of <2%. PMT nonlinearity is also unlikely to be a major (>2%) error source at the currents used for these measurements, since the ratio of the .5mm/.8mm and 1mm/1.8mm entrance/exit slit combinations remained constant over a wide range of PMT currents and were the same for both mini- and maxi-arcs.

3. Improper registration of the 1/2mm entrance aperture pinholes. As mentioned above, the 1mm aperture remained in place throughout the calibration but the 1/2mm pinhole had to be removed and replaced on numerous occasions. If improperly placed (it was taped over the 1mm pinholes) some of its area might be occulted (once it slipped causing an obvious measurement discrepancy!). The ratio between measurements in the small and large aperture configuration is just that expected from the relative aperture areas and the spectral resolutions, so we deduce that this is not a real error source.

4. Arc fluctuations. The NBS-5 arc appeared to be very stable and repeatable throughout the measurements. There is some evidence, however, that the MAXI-I arc suffered some instability and variations

in its spectral distributions. In the region of overlap between NBS-5 and MAXI-I calibration spectra we expected to be able to derive a wavelength independent ratio that can be used to scale the known MAXI-I spectral radiance to irradiance at the entrance aperture. This factor was found to have a wavelength dependence in the sense that ~8% more flux than expected from MAXI-I occurs at the longest wavelengths in the August data. Also, the ratio between the small and large aperture configurations is constant (and nominal) at long wavelengths, but shows an increase below ~λ1600 (more flux seen through the small aperture than expected) possibly indicating a change in spectral distribution between these two runs. The maxi-arc also showed visible and audible signs of instability. For these reasons we suspect that some systematic error may be present in the monochromator calibration below λ2000, but have no means of estimating its severity. Comparison of the June/July measurements with the August data is precluded because the monochromator entrance port MgF_2 window was changed in the interim (resulting in a factor of 15 improvement in throughput at λ1250!).

Our best estimate of the monochromator calibration uncertainty may be summarized as follows:

1. Above λ2000, where the calibration is reliant only on the NBS-5 arc, the measurement uncertainties are ±8%.

2. Below λ2000, this accuracy degrades with decreasing wavelengths, to ~±10% at λ1600 and ±15% at λ1250.

2.4.3 VSTOS Configuration and Alignment with NBS System

A special vacuum chamber was provided by MMDA for the purpose of VSTOS calibration. The chamber, pumped by an array of four sorption pumps and a CTI cryopump, was equipped with feedthroughs for the VSTOS control signals, lamp cables and thermistors and three windowed ports for inspection of VSTOS operation. To assure its cleanliness, the chamber was given an acid bath clean-up and a vacuum bake-out was performed before installation of the STOS. Witness mirrors were also employed. The STOS was mounted on a platform equipped with three jack screws for vertical tilt and translation adjustment and screws for translation in the horizontal and focus directions. Horizontal tilt was adjusted by loosening clamps that attach this entire assembly to the floor of the chamber. The VSTOS beam exited the chamber through a MgF_2 window (which was removed from the chamber and introduced into the arc beam during NBS monochromator calibration) to which a bellows was attached in order to seal the volume between the tank and monochromator entrance port window. This volume was flushed with argon during all measurements below λ2000Å. All measurements were made with the VSTOS under hard vacuum (chamber pressure $<2 \cdot 10^{-5}$T).

2.4.3.1 Alignment Method

Alignment of the VSTOS was effected in two steps: a crude alignment was first obtained by means of a laser beam and final adjustments were made by peaking up the monochromator signal. A He-Ne laser was initally aligned with the monochromator by adjusting its tilt until it shone through the centers of both entrance and exit slits and was reflected (in zeroth order) from the exact center of the concave grating. The STOS was then adjusted so that this beam was centered on the back of the secondary mirror support of the STOS inverted Cassegrain and was reflected, from a glass plate held flat against the STOS front mounting surface, back onto the monochromator entrance aperture. The distance between this mounting plate and the aperture was adjusted to be equal to that in the FOS calibrations configuration (34.8cm). The STOS was then prepared for vacuum operation (all lamp cables attached and carefully adjusted to assure that they would move freely and cause minimal torque on the carousel), the PMT replaced on the monochromator, and the glass plate removed from the front of the STOS. The STOS carousel was reset, then moved to the Pt-Cr/Ne #2 lamp position and the signal from a strong line maximized by a combination of small tilt and translation adjustments in both axes. This lamp was chosen for alignment purposes because of its relatively small and symmetrical image. The vacuum chamber was then closed, with the MgF_2 window and bellows installed, and evacuated. Finally, the operation of the carousel and all lamps was checked before proceeding with the calibration.

2.4.3.2 VSTOS Image Mapping

The image of each of the VSTOS lamps at the (1mm) monochromator entrance aperture was mapped during the August recalibration to determine the alignment sensitivity. Horizontal mapping was achieved by rotating the VSTOS lamp carousel by single motor steps, moving the image ~1mm per step. Vertical mapping was done by turning the jack screw under the monochromator entrance port tube, thereby raising and lowering the aperture, while tilting the entire monochromator. Vertical step size was ~.7mm. Changes in monochromator response due to the very small tilt as well as changes in the image intensity and spatial distribution due to variation of the source position relative to the VSTOS optical axis were assumed to be minor over the range of the mapping. Measurements were generally made near both the long and short wavelength ends of the calibrated spectrum of each lamp, to investigate wavelength dependences. Figure 2.1 illustrates the results. These data may be compared with the higher resolution mappings at visible wavelengths that were made when the VSTOS lamps were coaligned (see Appendix D).

Of particular interest are the strong wavelength dependence of the profiles for the argon and krypton lamps. The FUV profile for the argon lamp are asymmetrical and displaced from these at longer wavelengths, rendering this lamp less than ideal as an FUV calibration source. The Kr lamp image is considerably narrower as seen in the UV, and inverted at the center at short wavelengths, but the profiles are at least symmetrical and their center does not shift with wavelength. The images of the hollow cathode lamps and the hydrogen lamp exhibit no significant wavelength dependence. The narrow, symmetrical distribution for the Pt-Cr/Ne #2 lamp make it the ideal choice for

the alignment (peak-up) source, while the broad, nearly flat profiles for the P+Cr/Ne #1 lamp (with diffuser) make it most insensitive to alignment error and, as such, particularly useful as an absolute calibration standard.

2.4.4 VSTOS Calibration Method

As was indicated above, the monochromator was used in two configurations, with a 1mm entrance aperture and 1.8mm exit slit and with a .5mm aperture and .8mm slit. The larger aperture was used to measure all of the VSTOS lamps, while the smaller was used for the Pt-Cr/Ne #2 lamp alone, in order provide the increased spectral resolution which was required for the separation of sufficient lines in the rather dense line distribution provided by the hollow-cathode lamps. The attenuation produced by the MgF_2 diffuser on the #1 lamp precluded use of the smaller aperture for this lamp, hence its calibration suffers greater uncertainties due to poorer signal-to-noise ratio (lines shortward of λ1524 could not be measured) and blending. The exit slit width was empirically determined in each case by opening it until the measured flux from an isolated line (from the Pt-Cr/Ne #2 lamp) was maximized, then reducing it to just the point where the signal began to drop. (Scans were made through the line during this procedure).

Measurements below ~λ2200 were made with the volume between the monochromator entrance port window and the VSTOS chamber window flushed with argon. The critical flow rate was determined by observing the measured flux at short wavelengths while adjusting the rate (with a flowmeter in the line) and watching for absorption by air diffusing into the cell. Measurements were

subsequently made at flow rates significantly larger than this critical value. At wavelengths longward of λ2200, air was introduced into the cell, thereby providing an order blocking filter.

2.4.4.1 Line Source Measurements

The spectral pass band for each configuration is required for the calibration of the line source irradiances. This was measured by slowly scanning the isolated λ2930 PtI line and calculating its full width at half maximum intensity. The dispersion of the Seya-Namioka monochromator is not constant, however, so the resolution measured at λ2930 must be corrected for use at shorter wavelengths. This correction amounts to a 13% increase in Δλ at λ1200; a linear approximation is sufficiently accurate for Δλ computation at intermediate wavelengths.

Initial measurements of the line fluxes were made by scanning the region around each of the selected lines in order to determine the wavelength of peak signal and determine the degree of blending. Final line selection was based on the need for a sufficient number of line to provide adequate coverage over each of the UV grating ranges (~5 lines, evenly spaced was our goal), the relative amount of blending in the candidate lines, and their intensity.

The Pt-Cr/Ne lamps were allowed to stabilize for at least 15 minutes prior to calibration. Some variation (different for each line) does continue to occur after this warm-up period. The fluctuation is typically on the order of 5% per hour and is not asymptotic.

2.4.4.2 Continuum Lamp Measurements

The krypton, argon and hydrogen lamps were initially scanned over the entire range of the monochromator (λλ1150-3100) to determine which regions had sufficient flux to be accurately measurable and which portions of their spectra were relatively free of contamination by lines, which tend to be intrinsically variable and also effect the accuracy of the calibration transfer between instruments with different spectral resolution. The argon lamp was determined to be useful in the ranges λλ1200-1450 and λλ2200-3000; the krypton lamp in λλ1300-3100 and the hydrogen lamp in λλ1700-3000.

The stability and required 'warm-up' time of the continuum lamps were investigated during the May calibration, the latter by rapid rescanning of the spectrum, or a selected portion thereof, while the lamp stabilized after a 'cold' start. Variations in the UV fluxes were observed for all three lamps, but were not major (typically $\leq \pm 3\%$) after a half-hour or less of operation. The krypton lamp flux continued to drop at a slow rate (<2% per hour) from the level reached shortly after turn-on. The hydrogen lamp was disappointing in that it often required restarting after it spontaneously extinguished; such restarts often resulted in fluxes considerably different from those just before failure.

An attempt was made to provide a means of independently determining the state of lamp stability by placing a pair of silicon photodiode/op-amp devices in front of the lamp carousel, such that the integrated flux level of two of the off-axis lamps could be monitored. Despite the fact that the detector

windows were coated with sodium salicylate to extend their UV response, the behavior recorded by these monitors was generally not indicative of the UV flux variations measured with the NBS system.

The long term stability of each of the continuum lamps was quite disappointing. The UV fluxes from both argon and krypton lamps decayed steadily from use to use, always restarting at levels below that recorded just before the previous turn-off. NBS system degradation cannot be at fault for these decays because they occur at different rates and the Pt-Cr/Ne lamp fluxes remained very constant throughout each calibration. The hydrogen lamp was less predictable and, as mentioned above, its output was dependent on whether or not restarting was required (as was often the case). It was also discovered that repeatedly pressing the 'start' switch for this lamp could change the lamp flux, indicating that it can operate in a variety of modes.

2.4.5 VSTOS Calibration Results

A summary of the calibration results, including a log of the measurements, may be found in Appendix C of the Calibration Report, the informal NBS report submitted by Dr. Klose. The logs, in addition to the date, times and configuration for each run, also indicate the signal level at one or more wavelengths to demonstrate the repeatability of each lamp. Since these are raw signal (dark subtracted) measurements, the pre- and post-FOS calibration values cannot be directly compared, because of the replacement of the monochromator entrance assembly window between the May and August calibrations. Of particular note is the stability of the Pt-Cr/Ne #2 lamp throughout each run; the measured signal from all three lines included in the

logs is repeatable from day to day within several percent. This attests to the stability of the NBS system and the repeatability of the VSTOS carousel in addition to that of the lamp itself. The other hollow cathode lamp was not monitored so frequently and the diffuser was added in the middle of the May calibration, but those measurements which are available indicate that this lamp is also very stable over periods of tens of hours of use.

Unfortunately, this is not true of the continuum sources. The hydrogen lamp proved to be rather erratic and gave indications of several modes of operation which settle to different flux output levels. Generally, though, the levels reached after ~1 hour warm-up were within ±8% of the average, especially if a restart was not required. No systematic trend could be discerned. The krypton and argon lamps both exhibited a very clear trend toward decreasing equilibrium flux with continued use. For this reason logs of the lamp use were kept through the FOS calibration period with hope that a reasonably accurate interpolation to the actual flux levels at the time of the FOS APC could be made. Figures 2.3 and 2.4 illustrate the calibration histories of these lamps at wavelengths near the peak of their FUV continua and in the near UV. The trend to decreasing flux with accumulated lamp use is evident during the May calibration for both lamps and this trend continues during the August calibration for the krypton lamp. The argon lamp behaves more erratically (in the FUV) during the August calibration, and jumps up by about a factor 2.4 between 31 May and 7 August. Only a small increase is noted for the krypton lamp at a slightly longer wavelength, so the monochromator calibration is not likely at fault. (Also note that in August the Pt-Cr/Ne #2 lamp lines at λ1248 and λ1404 each show a <u>decrease</u> of ~30% from their

May levels.) At longer wavelengths (e.g. λ2300) the argon lamp flux increased by only 20% in the same interval, and proceeded to decrease monotonically during the August measurements, as in May.

It is obvious that the consistent degradations measured during the NBS calibration periods could not have persisted at the same rate while the lamps were used for the FOS APC; in fact, they seem to have recovered slightly during that period. Therefore, estimation of the flux at the time of FOS APC cannot be made by direct interpolation or extrapolation of the levels shown in Figures 2.3 and 2.4. It is unclear what degradation mechanism could be operating during the NBS calibrations; it may be dependent on duty cycle since the lamps were used sparingly with fairly long rest periods between APC measurement. No correlation with chamber pressure is obvious; e.g., the chamber was opened (to insert the diffuser on Pt-Cr/Ne lamp #1) and re-evacuated in the middle of the first NBS run but the fluxes do not mirror the resulting changes in operating chamber pressure.

The Pt-Cr/Ne lamps each suffered drops in the measured line fluxes from the May to August calibrations, with an average decrease of ~10% for the #1 lamp and ~23% for the #2 lamp. No correlation with wavelength is apparent. This is consistent with the variations seen during life tests performed on an identical lamp at the Johns Hopkins University in 1981, which showed flux changes as great as a factor 2 over ~1 Amp-hour of intermittent operation (at 10mA). The 'workhorse' #2 lamp, used for alignments and many tests of the FOS other than the APC, experienced ~1.5 Amp-hours of use (or ~15% of its expected life) in the interval between the May and August calibrations, while the #1 lamp logged ~.25 Amp-hours (both also operated at 10mA).

2.4.5.1 Uncertainties in VSTOS Calibration

In addition to the NBS monochromator calibration (sec. 2.2.2), the many sources of error described above must be accounted for in our estimates of the accuracy of the absolute VSTOS irradiance assignments. Following is an attempt to estimate these uncertainties.

1. VSTOS carousel repeatability and NBS system stability, including repeatability in positioning of the PMT. The maximum total error due to these is estimated to be less than ±3% from the repeatability of the Pt-Cr/Ne #2 lamp measurements which were made periodically throughout the calibrations.

2. VSTOS/monochromator alignment. The signal of a line from the Pt-Cr/Ne #2 lamp was maximized to within an estimated ±2%. This implies a maximum offset of less than 250μ which, in the worst case of the krypton lamp in the NUV, would imply a signal loss of <6% based on the image mapping shown in Appendix D. Flux loss due to tilt misalignment, independent of which lamp is in use, is less than ±2%.

3. Monochromator response to VSTOS beam. The correction factors derived from the monochromator mapping are subject to assumptions of uniform flux distribution over the VSTOS beam, size of the central obscuration and, probably of greatest importance, that the response at any point is the product of the responses on the horizontal and vertical axes

which intersect at the optical axis. We have no means of precisely determining these uncertainties but estimate a maximum tolerance of ±5% in the correction factor.

4. Monochromator pass band. Although this was measured to within ±2% at λ2930, it was later realized that the pass band is dependent on wavelengths, requiring a correction by 13% at the shortest wavelengths according to calculations. This was not empirically verified, however. This is important only for the spectral line sources (Pt-Cr/Ne lamps).

5. Signal-to-noise ratio, system non-linearity and chart reading errors. These are generally accurate to ±2% with the following exceptions due to lower S/N:

   - all argon lamp measurements : ±5%
   - Pt-Cr/Ne #1 $\lambda \leq 1723$: ±5%
     $\lambda \geq 1916$: ±3%
   - Pt-Cr/Ne #2 λλ1248,1404,1622 : ±3% (small aperture/slit configuration)

6. Lamp variability. This is probably the dominant error source for each of the continuum lamps, since their behavior is not consistent through the calibration period. We defer estimation of these errors to Section 3.3, where they are discussed in the context of the FOS APC.

With the exception of the effects of lamp variability then, the total uncertainty in our calibration of the VSTOS may be summarized as follows: all measurements above λ2000 are accurate to within ±11%, degrading to ±17% at the shortest wavelengths, with the error in all cases being dominated by the uncertainties in the absolute calibration of the monochromator response.

3. FOS APC

3.1 General Method

Absolute photometric calibration of the FOS was performed during the June through August 1984 test periods at MMDA, by using both the ambient and vacuum STOSs as sources of known irradiance at the FOS entrance apertures. With the aperture areas known, the photon flux at each wavelength of interest entering the FOS can be calculated and the efficiency, or quantum throughput (QT), measured by comparison of these fluxes with the resulting count rates. This QT should be the product of the optical efficiencies (reflectances of the mirrors, transmittances of the filters and prism, etc.) of the components along the light path and the quantum efficiency (QE) of the Digicon detector, if none of the flux entering the FOS is lost due to STOS misalignment or overfilling of the FOS optics. The geometry of the STOSs was designed to slightly underfill the FOS optics (in the same manner as the ST OTA), but losses will occur if small misalignments exist.

Some flux may also be lost due to diffraction by the smallest FOS apertures, particularly at long wavelengths. Dr. Richard Allen has made an estimate that such losses may be as large as 32% at λ6000Å through the A4 (.1") apertures. Preliminary results of calibration tests to determine the extent of light loss due to diffraction indicate that the wavelength dependence of the Allen estimates is correct. The actual aperture size measurements used for the APC reduction were made by integrating the flux seen through the various apertures (with the camera mirror) and thus represent a mean effective size over the wavelength response of the detector convolved with the spectral flux distribution of the FEL lamp. For the blue side measurements the wavelength for which the aperture size is representative is ~λ4000; for the red sides ~λ7000. (The latter measurements were made with the ASTOS FEL lamp current reduced to 4 Amps, causing it to be very red.) Assuming these mean wavelengths, the effective aperture areas, corrected for diffraction losses according to Allen's estimates, were used for the APC measurements made with the A4, A3 and B2 apertures. We estimate the uncertainty in the absolute aperture areas at ±5%, with the exception of the A4 apertures: their small size, relatively ragged perimeters and large diffraction loss corrections render these areas uncertain to ~10%.

All calibration data was taken in the standard spectrophotometric mode, with quarter stepping and an overscan of 5 diodes. The raw data were corrected for dead time (paired pulse correction) with time constants t_1 = -1.08(-5)s and t_2 = 1.92(-5)s, according to the relationship described by Ebbets (1985). In a few cases this correction is large (as great as 50%) but the majority of the APC data involve observed count rates below 10,000 counts/s/diode, where the correction is about 10%. The accuracy of the

correction is estimated to be within ±2% for observed count rates below 10,000, escalating to ±5% at 30,000 and ±10% for the few APC data points near 33,000 counts/s/diode. These uncertainties derive from the errors inherent in the paired pulse correction calibration, which relies on accurate knowledge of the relative aperture area. Efforts are currently being made to improve the accuracy of the count rate correction.

3.2 Ambient APC

The FOS QT was measured with the ASTOS in both June and August 1984. The alignment of the STOS with each side of the FOS was checked during the June calibration by successively occulting all of the beam except a small circular area at the beam edge, centered on each of the spider legs supporting the STOS occultation aperture disk. The deuterium lamp was used and maps of the 0.1 arcsec (A4) apertures were made with the camera mirror. If the STOS is significantly misaligned, the resulting signal from each quadrant would be different and the sense of the misalignment could be readily deduced. Prior to the June APC, the STOS was found to be in excellent alignment on the FOS blue side, with variations among the quadrants of less than 4%. A later check, after several STOS repositionings and immediately following the APC measurements, yielded less desirable results, with deviations up to 9% from the mean, but nevertheless indicating relatively small beam loss. On the red side, however, the results indicated significant misalignment the 'W' image containing only ~47% of the signal in the 'E' image, while 'N' and 'S' were essentially identical and ~15% less than 'E'. The diameter of the test aperture is 9.9mm, and the STOS occultation aperture diameter is 33.1 mm. We

can infer from these data that the fraction of the ASTOS beam lost on the red side was most likely between 10 and 20%. The large uncertainty in this estimate is due to effects of diffraction through the A4 aperture, which make the computation of beam loss unwieldy and dependent on wavelength and the true aperture size, since where the diffraction losses are large, we would expect the sensitivity to misalignment to be reduced. Similar calculations for the blue APC yield a beam loss estimate of 5 ±2%.

An attempt was made on 23 Feb 85 at LMSC to align the ASTOS on the red side with essentially the same technique, but utilizing the B3 aperture (for which diffraction losses are negligible) and the FEL lamp, operated at reduced current (4A). Considerable realignment was required to equalize the 4 quadrants. Spectra representing a subset of the standard APC procedure were obtained with the FEL lamp #179 at nominal current (8.01A). These spectra contained only ~.78 of the flux seen in the 'misaligned' August 84 spectra, independent of wavelengths from below λ3000 to above λ8000Å. Since internal caibration lamp spectra and flat-field LED exposures made subsequently produced results nearly identical with many previous tests (including those made in August 84), the instrument has not degraded and we can only conclude that the STOS alignment technique used here is faulty in some manner. The data obtained with the STOS in its original, nominally aligned orientation must therefore be taken at face value, but since some beam loss which we cannot quantify may indeed be present the efficiencies calculated from those spectra represent lower limits to the true FOS QT. In retrospect, the ASTOS might have been better used by removing the f/24 field stops and using the diffusing screen as a calibrated radiance source.

Comparisons of the raw data from the June calibration with those of the August run indicate that the FEL lamp measurements are very repeatable. The August spectra almost all appear to have count rates that are approximately 4% (±2%) greater than the levels of the earlier spectra, with no obvious or systematic wavelength dependence. This is consistent with the fact that the August measurements were made with the Digicon operating voltage at the flight values: 20.9kV (red) and 22.4 (blue), while the June data were obtained at 18.4kV. The exceptions are both August measurements of the H57 grating on the red side which show a loss of signal at both ends of the spectrum; the spectrum taken through the B2 aperture is very clearly missing the diode array with nearly half of the light lost at each end of the spectrum and 20% lost near the central wavelength. This same effect is also present in the A4 spectrum, and is interpretted as due to improper centering of the image on the diode array caused by the nonrepeatable positioning of the filter grating wheel. The wavelength dependence is due to the 'C' distortion inherent in the Digicon. Y-scans were made before each of the June APC spectra to determine the correct Y-base (to center the spectrum on the array). We have taken the June H57 A4 spectrum and scaled it according to the ratio of the count rates at the center of the spectra from June and August (1.03) to calculate the QT for this configuration. The August data are adopted directly for all other configurations.

The GS-179 FEL lamp was used for all of the APC measurements with the exception of the August calibration of the blue side when the GS-180 lamp was employed. Both lamps were calibrated at the NBS and very little difference exists in their respective irradiances; the GS-180 lamp is a bit hotter, but between λ2600 and λ8000, the differences are less than 3%. Diffusing screen

#2 was used throughout the APC. As mentioned in sec. 2.2.1, some uncertainty exists in the lamp current because of failure of the power supply, but this is minimal, affecting the irradiance by less than 2%.

The deuterium lamp measurements were much less repeatable than the FEL data and very obvious differences in both overall count rate and spectral distribution were present, especially in the blue side data. The August measurements showed as much as a factor 2 increase in count rate compared to the June data, particularly at wavelengths below λ2500, in both H19 and H27 spectra. The poor quality of their calibration (see sec. 2.2.2) and this non-repeatability has rendered the deuterium lamps of little value and we have elected not to treat these data further.

The count rates were determined generally to within ±2%, with some degradation in accuracy due to poor S/N at the blue end of the prism spectra (~±5% at λ3000 and ±10% at λ2600). Because of the large integrated flux of the FEL lamps and the wide range of sensitivity of the detectors (especially broad for the 'red' Digicon), some correction to the observed count rates for scattered light were required for measurements below ~λ3000. The contribution due to scattered light was determined in a fairly straightforward manner: a separate calibration procedure, designed to measure the light scattering properties of the FOS, was executed during the August ambient calibration period. Since this procedure made use of the ASTOS with the calibrated FEL lamps and a series of blocking filters to directly determine the amount of scattered light in both H27 and prism spectra on both red and blue sides, we need only scale these measurements according to the relative aperture sizes used for these and the APC spectra. A small additional contribution that does not scale with aperture size and is presumably due to light from the room

entering the spectrograph (at places other than the entrance aperture) and scattering directly to the detector, was measured by placing an opaque screen over the blocking filter. The resulting total correction for the H27 grating amounts to ~12% at λ2500, falling to <2% at λ2800, on the red side, and ~3.5% at λ2500 on the blue side. The prism corrections are larger: scattered light accounts for ~21% of the observed count rate at λ2600 and 4% at λ3000, on the red side.

The FOS QT was calculated from:

$$\begin{aligned} QT &= \frac{\text{count rate per diode}}{\text{photon rate per diode}} \\ &= \frac{hc}{\lambda} \cdot \frac{\text{count rate per diode}}{\text{photon energy flux per diode}} \\ &= 1.989(-7) \cdot \frac{R \cdot L - Rscat}{E_\lambda \cdot A \cdot d_\lambda \cdot a \cdot \Delta\lambda \cdot \lambda} \quad ; \end{aligned} \tag{3.1}$$

where R is the raw count rate per diode, L is the detector linearity correction (typically 1 to 1.1), Rscat is the estimated count rate due to scattered light, E_λ is the ASTOS spectral irradiance (W/cm^3) as reported in Appendix B of the Calibration Report, A is the true aperture area (cm^2), d_λ is a correction factor for diffraction losses through the aperture (1 to ~.6), a is the fraction of the STOS beam seen by the FOS as a result of STOS misalignment, and $\Delta\lambda$ is the FOS dispersion (Å/diode) at the wavelength of the measurement, λ(Å). Because of our inability to directly estimate the extent of ASTOS misalignment, as described above, 'a' has been set to 1 for these calculations (but see sec. 5.1). The results of the ambient APC measurements are displayed in Figures 3.1 and 3.2 for the red side and 3.3 and 3.4 for the blue side. Error bars reflect the uncertainties discussed above. Since the

ASTOS deuterium lamps proved useless and the FEL lamps were calibrated only above λ2500Å, no measurements of the H19 or L15 gratings were obtained with the ASTOS.

3.3 Vacuum APC

The FOS QT was measured with the VSTOS, on the blue side only, during the July 1984 thermal vacuum testing at MMDA. Three separate measurements were made, but because of a STOS misalignment problem only the last of these, on 22 July, is useful for direct QT determination. After the second measurement, mapping of the STOS image by single-stepping its lamp carousel showed that the image centers were about one carousel step CCW off the nominal position at which APC data was previously obtained. This is believed to be due to misphasing of the carousel and motor (see sec. 2.3.2.1) when the STOS was mounted and realigned with the FOS in the vacuum chamber. (A prior, careful alignment was lost when the adjustment shims were accidentally misplaced.) The final set of APC measurements was therefore obtained with the carousel always positioned one step CCW of the nominal. The image maps made during the APC, when compared with those obtained when the VSTOS was recalibrated in August, indicate that at this new position the VSTOS was fairly well aligned, so corrections for misalignment will be small.

The Pt-Cr/Ne #2 lamp is very sensitive to image misalignment, so we have inspected the image maps, made with the A3 aperture pair, to estimate how well the VSTOS images were centered on the FOS apertures. At the one step CCW position the upper aperture spectrum was about 9% brighter than the lower. Since the upper aperture has been measured to have ~2% greater area, the

misalignment in the direction perpendicular to dispersion is responsible for ~7% less flux in the lower aperture. The lower apertures are used for all of the APC spectra. The April VSTOS image mappings of this lamp (Hartig, 1984) can be used to infer in a self-consistent manner (by fitting the relative signal in the upper and lower apertures, given their 840μ spacing) that ~600μ of residual image displacement was present, nearly all in the 'Y' (perpendicular to dispersion) direction. Since the VSTOS was calibrated at a position for which the signal from this lamp is maximized, the (lower aperture) APC data should be corrected for the ~7% light loss. The diffused Pt-Cr/Ne #1 lamp is very insensitive to image misalignment, so no correction is required in this case.

Since similar mapping data, in both upper and lower apertures, is not available for the other lamps, it is difficult to make accurate misalignment corrections for these, especially since the image size and shape was found to have strong wavelength dependence for the argon and krypton lamps, and the argon and hydrogen lamp profiles are asymmetric. The following estimates of these corrections (fraction of calibrated VSTOS flux seen by the FOS) are based on interpolation of the (coarse) maps made at the NBS in August (Figure 2.1), assuming a 600μ displacement as suggested above:

Krypton lamp	NUV (λ2400):	.85 ± .06
	FUV (λ1440):	1.10 ± .05
Argon lamp	NUV (λ2300):	.79 ± .08
	FUV (λ1280):	.87 ± .06
Hydrogen lamp	λ-independent:	1.06 ± .10

The argon lamp corrections include adjustments based on the ratio of the signals measured at the nominal and one-step-CCW positions, since we are obliged to use APC spectra taken at the former carousel position because argon spectra were omitted from the 22 July recalibration due to lack of time.

The above discussion deals only with misalignment of the VSTOS image with respect to the FOS apertures; since the VSTOS produces an f/24 beam to nearly fill the FOS collimator, the APC measurements are also sensitive to VSTOS tilt. The original tilt adjustment was performed by placing a cover over the FOS collimator which masked all but a small area (a series of small holes) along one edge and adjusting the VSTOS tilt until the signal from each of four orientations of the cover (rotated in 90° increments) were about equal. The necessity of moving the carousel one stop CCW from its nominal position to recenter the images implies some amount of tilt misalignment. This is probably small; the fraction of the (centrally-obscured) beam lost due to the tilt caused by one carousel step, if the collimator is just filled, is about 6%. The collimator is nominally slightly underfilled and diffraction through the smallest apertures will cause an overfilling which reduces sensitivity to tilt, but the intermediate case of a small amount of diffraction (e.g. through the A3 aperture) may cause beam loss due to tilt to approach 6%. Because of the intractable nature of this calculation and uncertainties in the tilt misalignment (with the carousel in its nominal position) produced when the VSTOS was realigned, we will not attempt to apply a correction to the APC data.

The high degree of variability of the VSTOS continuum lamps was discussed in section 2.4.5 with regard to the VSTOS calibration. It was noted there that the non-systematic behavior of these lamps over the May-August interval

precluded attempts to correct for the variability by simple interpolation of the NBS and FOS measurements. In order to minimize the effects of lamp fluctuations, the 22 July APC measurements and the 7-8 August VSTOS calibration were adopted for purposes of determining the FOS QT. The krypton, hydrogen and Pt-Cr/Ne #1 lamps were essentially unused in the interval between these measurements and the #2 hollow cathode lamp was on for only several hours (for alignment of the VSTOS with the NBS system). In general, the earliest NBS scans were used, with exception of the hydrogen lamp, which operated at an anomalously low level on 7 August and the Pt-Cr/Ne #2 lamp, since the higher resolution measurements with the small entrance aperture on the monochromator, made on 8 August, were desired. This policy was dictated by the general degradation in the output of the argon and krypton lamps with accumulated operating time which is evident in both NBS calibration periods and the (much slower but unpredictable) fluctuation of the hollow cathode lamp line fluxes.

An estimate of the uncertainty in the QT due to lamp variability may be made by examining the spread in count rates for each of the FOS APC measurements of similar configurations. These measurements are not indicative of the variations produced by the lamps alone, since various corrections must be applied that are somewhat uncertain in themselves, for different Digicon operating voltage and aperture size and misalignment. Nevertheless it is apparent that the argon and krypton lamps did not degrade consistently with use during the T/V 3 calibration, as they did during each NBS/VSTOS calibration. Figures 2.3 and 2.4 show, in addition to the VSTOS calibration points, the relative signal at each FOS APC measurement, normalized to indicate the NBS system signal required if the FOS QT were just that predicted on the basis of the

individual component efficiencies. The relative consistency of these data suggest that the mechanism responsible for the degradation during the NBS runs is peculiar to those measurements and further recommends the policy of selecting the earliest possible VSTOS calibration data following the FOS APC.

As noted in section 2.4.5, the August calibration of the argon lamp at short wavelengths showed a factor 2.4 increase over the May measurements. This jump and the rapid, erratic changes recorded during the August run make the FUV argon calibration highly uncertain and we have chosen not to include these data in our estimates of the FOS QT. We estimate that in the NUV, however, fluctuations in the argon lamp output will contribute ±5% to the QT uncertainty, so these data are quite useful.

FOS count rate variations of ±7% were recorded for the krypton lamp at long wavelengths (H27), and only ±2% in the FUV (H13). The latter is probably an overly optimistic indication of the variability (only three measurements were made); we adopt ±5% as more representative.

The hydrogen lamp continued to vary unpredictably through the FOS calibration, with variations of ±10% for the vacuum measurements. Both measurements made during the ambient APCs showed an apparent decrease in the hydrogen lamp flux by nearly a factor of two; these are clearly inaccurate indications of the FOS QT and may be due to differing operating characteristics of the lamp, depending on whether it is used in vacuum or at ambient.

The Pt-Cr/Ne lamps both show a general trend toward decreasing line flux with usage, although this is not uniform and varies from line to line. As an example, the #2 lamp output from the λ2930 line decreased by ~7% from 22 July to 28 August, while the λ2733 line remained constant and λ2487 increased by 20%. This lamp logged approximately 17 hours of operation between these meas-

urements, while only ~4 hours of use elapsed between the adopted FOS APC and NBS calibration or 8 August. We estimate the uncertainty in the QT due to fluctuations in these lamps at ±5%.

The FOS QT was calculated from the continuum source measurements, in the same manner as for the ASTOS APC, so equation 3.1 applies, except that the VSTOS irradiances have been calculated in $\mu W/cm^2 nm$ (instead of W/cm^3) requiring that the conversion constant be changed to 1.989(-8). No scattered light corrections were required for the vacuum APC spectra.

The line source measurements are reduced with:

$$\begin{aligned} QT &= \frac{\text{count rate in line}}{\text{photon rate in line}} \\ &= \frac{hc}{\lambda} \cdot \frac{\text{count rate in line}}{\text{photon energy flux in line}} \\ &= 1.989(-9)\ \frac{\Sigma_{\Delta\lambda}\ (R \cdot L)}{E_{line} \cdot A \cdot d_{\lambda} \cdot a \cdot \lambda}\ ; \end{aligned} \qquad (3.2)$$

where E_{line} is the line irradiance in $\mu W/cm^2$ and the other quantities are as defined above. Since the FOS resolution is generally much higher than that of the NBS monochromator and the spectral lines are not well isolated in many cases, the FOS count rates are summed over the pass band used for the NBS measurements. Since the NBS resolution exceeds that of the FOS prism for λ>~2500Å, some correction to the long wavelength line rates was required. The correction factor to be applied to the prism data was estimated by taking the ratio of the counts in the NBS passband to the counts within the FOS prism resolution width (centered on the line wavelengths) in the Pt-Cr/Ne #1 H27 spectrum. The corrections were 20% or less and we estimate that their contribution to the QT uncertainties is minor. Because of the excessive blending of the λ1622, λ1670, λ2263 and λ2357 lines, combined with the small, but non-

negligible wavelength uncertainty for both the NBS and FOS calibration spectra (especially for L15 and the prism), the estimated errors in the QT determined at these wavelengths are somewhat greater than for the better-separated lines.

The results of the vacuum APC of the FOS blue side are shown in Figures 3.4 through 3.8. Error bars reflect the uncertainties discussed above.

4. FOS Component Calibrations

Each of the FOS optical components, gratings, mirrors, filters and prism were measured at the Johns Hopkins University (JHU) Physics Department to verify their performance and allow selection of the elements to be used in the flight instrument. The quantum efficiency of the Digicon detectors was determined by their manufacturer, EVSD, for the same purposes. We can employ these measurements of the selected components to determine the expected overall FOS efficiencies. It is the purpose of this section to present the predicted efficiency data, with estimates of their uncertainties, so that these can be compared with the end-to-end measurements previously discussed. Details of the individual component measurements are beyond the scope of this report.

4.1 Optical Components

The JHU optical component measurements employed several separate facilities. Two comparators, one for measurements above λ3000 and one for the UV ($1150 < \lambda < 3100$), were configured to illuminate the dispersers with collimated light at the proper angle of incidence. These utilized PMT detectors on

translating stages preceded by exit slits at the proper distance from the comparison and test mirrors and gratings, and faithfully reproduced the optical configuration of the FOS. The comparators were preceded by ½m scanning Ebert monochromators, illuminated by hollow cathode lamps (Pt-Cr/Ne and Cr/Ne were used in the visible and Pt/Ne in the UV). Transfer optics and apertures were used to produce a beam that uniformly illuminated the test piece such that it is just underfilled, again simulating the FOS conditions. Plane polarizers, a polymer film type for the visible and one employing a single Brewster's angle reflection off bare LiF for the UV, were also incorporated in order to measure the optical efficiency for light polarized in the planes perpendicular and parallel to the grating rulings. The comparators allowed the direct cross-calibration of a test mirror or grating with a reference mirror of the same dimension and focal length, which results in very small errors because the beam path is identical for both pieces.

The reference mirrors were evaluated in separate facilities for UV and visible reflectivity measurement, each carefully configured to minimize errors due to beam size and nonuniformity, PMT photocathode nonuniformity and sensitivity to orientation, as well as source variations. Different configurations were employed for each mirror type: plane, grazing incidence, collimators (1m focal length) and camera and spherical (½m focal length).

For all of the measurements analog PMT currents were recorded on calibrated chart recorders and these data were manually reduced. The measurements were performed chiefly by Mr. Charles Bowers under the direction of the author, and the data were reduced by Mr. Richard Pembroke. Comments on the calibration of each component type, with estimates of their uncertainties, follow:

4.1.1 Concave Reference Mirrors

The UV and visible reflectivity measurements, each made with entirely distinct apparatus in different configurations, agree quite well at their juncture near λ3100Å (although little or no overlap in the wavelength coverage exists). For the collimators, the agreement is within 2%. A rise of ~5% occurs from the UV to visible reflectances of the spherical mirrors but this may be due, at least in part, to a real feature in the reflectance curve. The measured reflectance curves are also in agreement with that calculated from the optical constants, assuming a 250Å MgF_2 coating on Al; the measured values lie typically ~5% below theoretical and show a departure from this trend only in the vicinity of λ1650 where an anomalous dip in reflectance is known to occur for these coatings. We estimate that the absolute reflectivities of these mirrors, against which all the other mirrors and gratings have been evaluated, is determined to within ±5% of their true values, over the entire wavelength range of the measurements.

4.1.2 Collimators

These were, in general, calibrated by comparison with the UV and visible reference collimators. The statistical errors incurred by this comparison are small, estimated at ≤2%, except at λ1199 (±8%) and λ7943 (±7%). The measurement uncertainty is therefore essentially that of the reference mirror. An exception is the red side collimator, which was used as the visible reference mirror and, as such, was directly calibrated.

4.1.3 Gratings

The gratings were measured by comparison with the UV and visible spherical reference mirrors. Care was taken to assure that the proper angles of incidence and diffraction were used; alignment was performed by measuring the zeroth-order reflection geometry with the aid of a laser. In addition to the overall, first-order reflectance (with the grating nearly filled), the efficiency of each panel of the (multipartite) gratings was measured, with a stopped-down beam. Although no central obscuration (as present in the actual FOS beam) was utilized in the full-illumination measurements, the resulting 'error' is negligible since the efficiency of each panel does not deviate strongly from the mean. The H13 and H19 gratings were replaced in the FOS and their spares remeasured before mounting; the measurements are in excellent agreement (<2%) at points near the center of their wavelength coverage ($\beta \approx 0$), but some significant disagreement is present at the wavelength extremes, especially for H13 at points below λ1248. The latter may be due to some real degradation, amounting to ~15% at λ1219, presumably due to surface contaminants, despite the care taken in grating handling and the fact that the gratings were stored in their special, O-ring sealed containers in the intervening two years. The other discrepancies may be at least partly due to slightly different grating alignments, with corresponding shifts of the blaze wavelength, which would be most apparent at the larger diffraction angles, where the efficiency falls rapidly as β departs from the blaze.

4.1.4 Prism

This was measured as an assembly after the prism was bonded to the spherical mirror and was treated in the same manner as the gratings. Again, the agreement between UV and visible measurements is good (.81 at λ3065 with the UV monochromator, and .805 at λ3323 with the visible). Reasonable agreement with the measurements was obtained by an attempt to calculate the efficiency using the optical constants of the MgF_2 A/R coating and sapphire, although some variance exists in the published data (Pembroke, 1983).

4.1.5 Grazing Incidence Mirrors

These were measured directly (not with respect to a reference mirror), although for the visible measurements use was made of a pair of auxiliary flats and a beam-splitter in a double-pass arrangement that permitted the single PMT to remain stationary. One flat returned the beam reflected by the grazing mirror and the other reflected the beam when the grazing mirror was removed; both were used at normal incidence. Because the beam made two reflections at the proper angle of incidence (78.5 degrees, chief ray) the accuracy is improved. However, we note that although care was taken to illuminate approximately the same area of the mirror as is used in the FOS, a central obscuration was not present and the ±1.2 degree range in angle of incidence presented by the OTA f/24 beam was also not exactly duplicated since the test beam was nearly collimated. Nevertheless, we expect that these differences incur only very minor errors. The UV measurements were made in a direct fashion, and excellent (<2%) agreement between these and the visible

reflectance near λ3000Å was again achieved. Each face (red side and blue side) was measured. Separate measurements were made with plane polarized light in directions perpendicular and parallel to the plane of incidence, showing the expected substantial polarization, especially in the red. These results compared, within 5%, to reflectances calculated from the optical constants for Al and Al_2O_3, assuming a 45Å thick growth of the latter on the 'aged' bare Al coating (Pembroke, 1984).

4.1.6 Filters

The order blocking filters were measured at JHU only in the UV (λ<3000Å). With the exception of the filter used for the H27 grating (MgF_2 anti-reflectance coated fused silica), the measurements lie below the nominal filter cut-off and provide determinations of the amount of filter leak. Transmission measurements of the anti-reflectance coated colored glass filters provided by Acton Research Corp. (ARC, the coating vendor) were made at very high S/N and variations among pieces of the same type are very small. The ARC data for the H27 filter are within 1% of the JHU measurements, providing confidence in both sets of data.

4.2 Digicon Q.E.

The efficiency of the flight detectors has been determined at Electronic Vision Systems Division (EVSD) of Science Applications International Corp., where the tubes were constructed. A fairly comprehensive summary of the test results for each of the FOS program Digicons, including the F-3 (red) and F-7

(blue) flight-selected tubes, has been previously prepared (Beaver and Harms, 1984).

Briefly, the QEs were determined by comparison with a pair of standard photodiodes, the absolute efficiencies of which were provided by their vendors (EMR and EMI). The comparison is generally indirect for the visible measurements; an intermediate standard Digicon was first calibrated in current mode using the photodiode, then in turn used to calibrate the tube under test in either current or photon-counting mode. Two sets of apparatus are used to measure the UV and visible portions of the spectrum, with substantial overlap in their respective coverages. Each employs a monochromator, preceded by line (UV) or continuum (visible) sources, which is used to illuminate both a standard detector and the Digicon under test. The visible standard is an EMI 9715 QAM vacuum photodiode and an EMR 543-09-00 photodiode, whose calibration is traceable to the NBS, is used in the UV. The UV apparatus makes use of a secondary standard PMT, sensitive to visible light, to monitor the brightness of a phosphor screen, which can be moved into the beam behind the monochromator exit slit, to normalize the beam fluxes between comparison measurements of the photodiode and test Digicon. Four lamps are used for the UV emission line measurements: Xonics hydrogen (λ1216), Xonics krypton (λλ1236, 1460), Scientific International xenon (λ1473) and a mercury pen-ray (λλ1850, 2537, 3131, 3650 and 4047). In addition to the current mode QE-measurements made at each of these wavelengths, a photon counting mode determination was also made at λλ1216, 1850 and 2537. The agreement between the QE determined in each mode for the F-7 digicon is within 5%.

The only UV QE measurements that are available for the flight detectors were made at the time of delivery in April 1981 (red) and July 1981 (blue).

Subsequent tests have been made with the visible apparatus (λ>3600Å), however. For the blue F-7 tube the measurement in April 1984 is generally in good agreement with the delivery values, but with some degradation of the red response indicated. The red F-3 tube data are not so easily interpreted: discrepancies ranging from a factor of 1.5 to 2 occur in the remeasurements of July 1983 and March 1984. These lie above and below the delivery values, respectively. We suspect that a large part of the discrepancy may be due to the particularly high ion count rate exhibited by this tube, which produces an apparent enhancement of the efficiency near the tube center when the photocathode is illuminated over a wide area. This effect was as large as ~50% in the most recent EVSD measurements and was accounted for by measuring the QE away from the center. The anomalously large QEs reported in July 1983 may be at least partially the result of this ion count enhancement, although the ion count rate was measured to be substantially smaller at that time. Since no recent measurements have been made below λ3600, we assume that the approximately wavelength-independent ratio of the March 1984 to delivery values (~.8) is valid at shorter wavelengths and derate the UV QE measurements accordingly. The 1984 remeasurements of both tubes were made with respect to the F-2 Digicon, which was calibrated (in current mode) against the EMI photodiode at the same time. These data should therefore provide an excellent cross-calibration of the two flight detectors even if systematic errors, such as degradation of the reference photodiode QEs, are present. EVSD has recently obtained another calibrated EMI (visible) photodiode and has found that the older standard has not degraded significantly.

A systematic error in the EVSD QE measurements at the shortest wavelengths was recently discovered as a result of comparing efficiencies measured

by both EVSD and the NBS for several different detectors. The EVSD evaluation of standard photodiodes, which it manufactures for the NBS, has produced consistently higher QE than the subsequent calibration at the NBS. This discrepancy amounts to ~30% at λ1236, dropping to ~9% at λ1460 and <2% for λ>2000Å. The HRS Digicons were also measured at the NBS, GSFC and EVSD; for the CsTe tubes the discrepancy is much the same, with NBS and GSFC evaluations in good agreement. The HRS CsI Digicons do not show such a marked discrepancy, however.

The EVSD UV standard photodiode has just been re-calibrated (January 1985) and shows only an ~3% degradation in its QE at λ1216 from its 1978 value; furthermore, mapping of the diode photocathode area indicated that spatial variations in its response are fairly small, so beam 'footprint' considerations are probably not the major cause of the EVSD/NBS discrepancies. The problem is most likely caused by scattering of long wavelengths, since the sources in question produce significant fluxes in the NUV. The EVSD measurements of the HRS CsI Digicons, which have a very restricted range of sensitivity (essentially blind to the NUV) and are therefore less susceptible to QE measurement errors as a result of scattered light, were in considerably better agreement with the NBS data. We have scaled the EVSD measurements below λ2000 according to the average ratio of NBS to EVSD QEs of three photodiodes which were recently measured.

An estimation of the uncertainties in the EVSD measurements can be made by inspection of the QE history of the F-2 tube, for which seven sets of data are reported in the report by Beaver and Harms (1984). The spread in these measurements, which do not exhibit a clear temporal trend (except for the original delivery data of 1981 which show a more sensitive red response), is

about ±10% at λ4000Å degrading to ~±30% at λ8000Å. Although such data is not available for the UV measurements, we estimate the uncertainties at ±30% at λ1216, where the signal-to-noise ratio is poor and corrections of that order have been applied. The uncertainty improves to ±10% at λ2537, since the UV and visible measurements, which involve entirely separate apparatus, generally agree to within 10% where they overlap.

4.3 Predicted FOS QT

The expected efficiency of each FOS observing configuration is the product of the reflectivities of the grazing mirror, collimator and disperser, the transmittance of the order blocking filter (if present), and the Digicon QE, assuming proper alignment of these components and the absence of beam occultation (e.g., by misplaced baffles). The predicted QT values have been calculated, based on the measurement described above, and are shown in Figures 3.1 through 3.9, as dashed curves. The error bars represent the uncertainties in the individual component measurements, added in quadrature.

Cubic spline fits to the efficiency data were adjusted to remove the amplification of measurement statistical error that is typical of this type of fit and to produce reasonable extrapolation of the data where required. We note that, particularly for the Digicon QE in the UV this is a somewhat arbitrary process, since this region is poorly sampled and no recent measurements are available, resulting in a reduction in the level of confidence for the FUV efficiency predictions, especially on the blue side.

5. Analysis and Conclusions

A summary of the detailed error analysis included throughout the preceding sections is presented in Table 5.1. All of the error sources for which we are able to make a reasonable estimate of the contribution to the overall error budget are included. The error bars due to NBS system calibration and its transfer to the ASTOS have been combined since the NBS Report of Calibration does not include a breakdown. For some of the table categories, the indicated range of error represents a variety of individual measurements (with each of the VSTOS lamps and of several disperser/aperture combinations). The error bars plotted in Figures 3.1-3.9 reflect the tabulated estimates for each measurement and for the 'predicted' QT errors. Omitted from this summary table is the possible systematic error due to misalignment of the ASTOS with the FOS (see section 3.2), which may have a significant effect on the results, but for which we have no direct means of evaluation.

Table 5.1 Summary of Errors

	Error (%)					
	VSTOS			ASTOS		
	1250Å	1500Å	2000Å	3000Å	5000Å	7000Å
NBS Standards & Equipment	15	10	8	8	6	6
Transfer to STOS	8	7	7			
Transfer, STOS to FOS	12	11-18	11-22	7-15	6-11	6
RMS Measured QT	21	16-22	15-24	11-17	9-13	9
Predicted QT Error	32	18	16	16	15	20

5.1 Intercomparison of Results: General

We can exploit the partial redundancy of many of the APC measurements to gain further insight concerning the systematic errors that may be present thereby permitting a better estimate of the true FOS QT. An obvious starting point is comparison of H27 and prism QTs on the blue side, which were measured with both the ambient and vacuum STOS. We find that the VSTOS measurements lie, on the average, ~30% above the ASTOS-produced QTs. This is contrary to expectation that the VSTOS, which produces a rather small image at the FOS apertures, would be more difficult to align than the ASTOS and therefore be more susceptible to beam loss due to residual misalignment (see also the discussion of VSTOS alignment problems, sec. 3.3). Nevertheless, the apparently straightforward ASTOS alignment check method has recently proven doubtful as a result of an attempt to align the ASTOS with the FOS red side that resulted in 22% less measured flux than in the 'misaligned' condition (see sec. 3.2). It seems reasonable to assume that losses of the same order may well be present in the nominally aligned blue side ASTOS spectra.

We may also compare the blue side ASTOS measurements of H27, H40, H57, L65, and the prism with those on the red side. As noted in section 4.2, the blue and red detectors were measured in the visible region against the same transfer standard Digicon within a short period of time and should therefore be well calibrated with respect to one another. The blue and red collimators were cross-calibrated (since the red side collimator was used as the reference mirror for those measurements) and each side of the grazing mirror, although separately measured, can be assumed to be well known with respect to the other since the measurements were made in exactly the same manner (and little dif-

ference in reflectivity was seen, as expected). Except for possible misalignments of the ASTOS or the FOS components, or beam vignetting by improperly placed baffles, etc. the APC measurements for each disperser should be nearly identical with respect to the predicted QTs. Rather, we find that the red side QTs more closely approximate the predicted values, again possibly indicating blue side ASTOS misalignment losses of ~20%, if the red side were perfectly aligned, and even greater losses if some red side misalignment was also present.

The majority of the discrepancy between the predicted and ASTOS-measured QTs is most likely due to some form of misalignment or beam vignetting since the ratio of measured to predicted efficiencies shows little global wavelength dependence, although this ratio does vary slightly over the wavelength range covered by some of the dispersers. It seems eminently reasonable, then, to normalize the blue ASTOS measurements to the VSTOS data for H27 and the prism in order to make our best estimate of the true FOS efficiencies. The alternative is to discount the quality of the NBS VSTOS calibration at the long wavelengths, where it is most accurate. At the wavelengths in question, the VSTOS irradiance calibration is tied most firmly (although by several intermediate standards) to the same standard used for the ASTOS calibration (see sec. 2.4.2.1), since the argon mini-arc was calibrated against an FEL lamp irradiance standard with FASCAL pedigree, in the NUV. The relatively good agreement (well within the errors expected from lamp fluctuations) demonstrated by the measurements with each lamp -- representing a variety of count rates, utilizing several different entrance apertures and including both line and continuum spectra -- lends further credence to the VSTOS H27 and prism results. Because the VSTOS was aligned with the NBS monochromator by maximizing the signal

(sec. 2.4.3.1), the irradiances could not have been significantly underestimated by beam loss due to misalignment. These arguments for the veracity of the VSTOS measurements are of course not compelling, since a number of transfers and corrections were involved and unidentified systematic errors may exist; however, we have no evidence that the measurements are less accurate than indicated by the error bars, whereas the ASTOS alignment is clearly questionable. At the shorter FUV wavelengths, a weighted mean of the VSTOS measurements is adopted, while the ASTOS QTs, normalized to the VSTOS results for H27, are used at longer wavelengths on the blue side. This approach brings the blue and red QTs, relative to those predicted, into reasonable agreement. The measured efficiencies generally lie at about 75% of the predicted values, such that the error bars of the predictions overlap those of the measurements.

5.2 Local Features and Anomalies

The measured efficiencies show some local departures from this global trend that merit further discussion. Of the ASTOS measurements, the L65 QTs toward the short wavelength end of its range on both red and blue sides appear to be somewhat lower, with respect to the predicted values, than the other components. The prism also appears relatively inefficient on the blue side (but not the red). The L65 discrepancy appears due to differences in the grating orientation in the FOS and for the JHU measurement set-up, since the drawing specifying the grating angles and blaze direction that was available to the JHU personnel was in error.

An explanation for the reduced efficiency of the prism on the blue side (as compared to the red) is somewhat more elusive. The count rates near the response peak in the June and August APC spectra for the prism appear to compare within ~5%, the August rates being the larger (as expected, due to the higher Digicon operating voltage). A more detailed comparison is precluded because the June data (for this exposure only!) were not properly recorded on tape. However, the shape of the spectrum through the upper aperture of the 0.1 arcsec ('A4') pair deviates considerably from that through lower in both the June and August spectra, with deviations between the two as large as 30%. Also, both spectra show multiple small-scale features not seen in the red-side spectra. A possible explanation is that the photocathode suffers some non-uniformity (or a small smudge or particle is present on the detector window) in the very small area over which the prism spectrum extends. This deserves further investigation as the flat fielding data are reduced in the near future. No attempt at flat-fielding the APC spectra has been made; the purpose of this exercise is to determine the overall FOS absolute efficiency on a fairly coarse scale.

For the VSTOS measurements we first note that in general the agreement among the QTs resulting from spectra of each of the five lamps is well within the errors expected from lamp fluctuation (see sec. 3.3). Noteable departures from this trend are the hydrogen lamp results at long wavelengths, which tend to drop below the other measurements increasingly with wavelength. A large part of this discrepancy is probably due to a real change in the spectral distribution of the hydrogen lamp, although such differences are not evident in the pre- and post-test NBS calibrations of this lamp. However, as indicated in sec. 3.3, this lamp seems to be particularly susceptible to output varia-

tions, possibly dependent on its environment and orientation. The PtCr/Ne #1 (diffused) lamp measurements also appear a bit lower than the mean of the others, especially for the lines below λ1800 in the H19 and L15 spectra. We suspect that this may be due to improper matchings of the NBS and FOS spectral resolution, perhaps combined with some loss of signal in the L15 spectrum, due to nonrepeatability of the FOS filter/grating wheel. The latter may be inferred by noting that the PtCr/Ne #1 measurements match the other lamps quite well in the H19 (above λ1800) and prism spectra in the same wavelength region, so their relative calibrations are accurate. The former may be a problem because of the high line density of the Pt spectrum, the poor resolution of the NBS measurements and the use of a rectangular (simple binning of the FOS spectra over the NBS $\Delta\lambda$) approximation to the true NBS monochromator resolution profile.

The VSTOS QTs, when viewed relative to the predicted values, show two noteworthy features: a sharp, high efficiency peak near λ1650, and a broad, shallow dip in the measured efficiency about ~λ2000Å. These features are not peculiar to a single disperser; the λ1650 feature can be seen in H13, H19 and L15 and the λ2000 dip in H19, H27, L15 and the prism. Inspection of Figure 3.8 (L15) shows that the former anomaly is due to the lack of the predicted efficiency dip in the measured QTs. This dip is known, however, to be a typical feature of Lα-optimized MgF_2/Al coatings, such as those used on the FOS collimators, FUV gratings and the mirror used with the prism. The depth of the feature in the predicted QT curve is not abnormal for two such reflections, although this varies considerably and has been correlated with the degree of surface roughness of the substrate. The absence of this dip is therefore quite unusual, and we can offer no ready explanation.

The dip in the ratio of measured to predicted QT at λ2000 is less prominent and, if the λ1650 feature were not present, it might be seen rather as a general decrease in efficiency with wavelength below ~λ2600. In either interpretation, the dip may be construed as a manifestation of some degree of surface contamination. In particular, a broad reduction in efficiency about λ2000 is a signature of surface contamination for Lα-optimized (250Å thick) MgF_2 over Al coatings, since the MgF_2 layer is of quarterwave thickness at ~λ2000 causing a greater degree of coupling to the surface contaminant at those wavelengths (Heaney, et al. 1977, Hass and Hunter 1970). In any case, the implied contamination in not gross; the ratio of the measured to predicted QT is nearly the same in the FUV as in the visible.

5.3 Final QT Estimates

With the considerations mentioned above in mind, we proceed to make our best estimate of the QT for each FOS configuration. For the blue side VSTOS results, the mean of the individual measurements made with each lamp, weighted inversely with the estimated uncertainty, was taken and a smooth curve drawn through these points. Extrapolation of the data was required below ~λ1300Å for the H13 and L15 gratings. The single measurement of H13 at λ1248 appears exceptionally high (at 86% of the predicted value), so our extrapolation lies about 15% below this value at ~70% of predicted, which is representative of the measurements over most of the spectral range of that grating.

The blue side ASTOS QTs were normalized, as described in section 5.1, to bring the H27 measurement into agreement with the VSTOS values. Since the shape of the H27 efficiency curves from each STOS match in the overlap region

(λλ2500-3000Å), only minor smoothing was required to yield a continuous QT curve. However, a 15-20% discrepancy remains between the VSTOS and ASTOS measurements of the prism, indicating (again) that the latter measurement is peculiar. Nevertheless, since a clear explanation for the low ASTOS result is currently lacking, we have elected to smooth the data through the overlap region, adopting the measurements outside that region without further major adjustment. The slope of the QT curve in the λλ2600-3000Å interval is likely to be somewhat incorrect as a result. Minor adjustments (not exceeding 2%) have been made to the ASTOS measurements in a few places to smooth the result, since measurement error can produce local variations of this magnitude.

The red side ASTOS measurements have generally been adopted directly, again with minor local smoothing. Since no measurements were made below λ2500Å on the red side, we must estimate the efficiency of L15 and H19 and the blueward portions of the wavelength ranges of the prism and H27 by assuming the predicted values are accurate relative to one another (as argued in section 5.1) and scaling the blue side VSTOS results accordingly. This results in some discontinuity in the region of overlap (λλ2500-3000Å) between the direct ASTOS measurements and the inferred UV values. Although the shapes and slopes are reasonably well matched, the H27 measurements fall ~10% below the inferred values, while the prism measurements are ~15% high. The latter is due partially to the anomalously low blue prism measurement (see above), but in both cases the agreement is well within the errors in the determination of the predicted red QTs relative to those on the blue side and the APC measurement errors. The (more uncertain) inferred values for the short

wavelengths have been normalized to the measured QTs in order to preserve the shape of the efficiency curve; small residual discrepancies were removed to produce a smooth curve.

The final estimated QTs are presented, with the predicted values superimposed as dashed curves, in Figures 5.1 through 5.4. Error bars representing our estimates of the interval in which the true FOS QT must reside are included. Appendix A contains tables of these estimated QTs.

5.4 Conclusions

The primary conclusion which we may draw from the APC data here presented is that the FOS is in good condition, with high sensitivity over its entire spectral range from the far UV to the near IR. Each of its dispersers and both Digicons demonstrate efficiencies that are a large fraction of those expected on the basis of measurements of the individual components. Furthermore, these predictions and the "end-to-end" APC measurements are generally in agreement within the estimated limits of the measurement errors associated with each.

Nevertheless, our best estimates of the system QTs are in general about 20-25% lower than the predicted values and little global variation in their ratio is present over the entire wavelength range, on either the red or the blue side (although the red QTs in the FUV were not directly measured). If this degradation is real, the average loss in reflectance or transmittance of the four to six exposed optical surfaces used for any particular configuration is 4-6%. This is not unreasonable, especially since the optics have previously been noted to be less than pristine (e.g. Herzig, 1984).

Some part of the difference between predicted and measured QT may well be due to STOS misalignment, however. Because of the close match of the output beams to the focal ratio of the FOS, inaccurate alignment of each STOS with the FOS is a major (and difficult to quantify) source of uncertainty in the QT determinations. Because the alignment of the STOSs with the NBS calibration facility was either very insensitive (ASTOS) or performed by maximizing the signal (VSTOS), and since their alignment with the FOS was both critical and difficult to perform and check, underestimates of the true FOS QTs are likely to have resulted. The evidence for such misalignment of the ASTOS on the blue side was considered convincing enough to warrant normalizing those data to the VSTOS measurements.

A wavelength-independent reduction in system efficiency can also be the result of some internal misalignment of the FOS optics, such as a baffle vignetting the beam or improper tilt of the collimator such that the beam partially misses the gratings. An inspection of the blue side optical train just prior to delivery to LMSC, although performed under less than ideal conditions, revealed no obvious obstructions or misalignments that could account for losses as great as 20%. Smaller effects cannot be ruled out on the basis of that inspection.

If the preflight schedule permits any further evaluation of the FOS efficiency, measurements should be performed in such a manner as to reduce the uncertainties due to misalignment. One such technique is the utilization of two beam focal ratios, one clearly underfilling the FOS optics (e.g. f/30), thereby reducing sensitivity to both alignment and diffraction by the smaller apertures, and the other filling the optics at f/24. The latter should be used to align the STOS by maximizing the signal; a small effort to provide a

reasonable way to articulate the STOS would aide this greatly. An alternative technique for the ASTOS is to use its diffusing screen as a calibrated radiance source by removing the field stops between the screen and the FOS apertures.

We conclude by reiterating that the FOS has been found "healthy" and free from any major debilitating contamination, and can be expected to perform efficiently in each of its observing configurations.

We have attempted to acknowledge the particular efforts of the main contributors throughout this report, but many others have provided general support for the laboratory APC of the FOS. The FOS group at MMDA, headed by L. Ripp and J. Vellinga, supplied the ASTOS and VSTOS and the technical and logistical support required to perform all stages of the calibration measurements. The NBS calibrations were chiefly performed by Drs. J.Z. Klose and J.M. Bridges (VSTOS) and J.H. Walker and D.A. McSparron (ASTOS), with Dr. H. Kostkowski providing consulting expertise. The FOS APC data were obtained with the able assistance of G. Strein (MMDA), K. Bilitch, R. Bentley and T. Gasaway (UCSD) and J. Fragola (Fairchild), and were reduced with the aide of D. Lindler and J. Wheatley. The individual optical component measurements were largely the result of the careful efforts of Dr. C. Bowers and R. Pembroke, under the auspices of Dr. A. Davidsen (JHU). Dr. E. Beaver, L. Acton and J. McCoy (EVSD) were responsible for the Digicon detector efficiency determinations. Finally, the authors wish to acknowledge the essential contributions of J. Ryan and Dr. P. Hintzen (GSFC), Dr. J. Koornneef (ST ScI), and the FOS Investigation Development Team, headed by PI Dr. R. Harms.

REFERENCES

Beaver, E. and Harms, R. 1984. "Faint Object Spectrograph Detector Report", April 1984, to STPG.

Ebbets, D. 1985. "Calibration of the HRS Paired-Pulse Effect", ST ScI HRS-CAL/006, January 15, 1985.

Harms, R. et al. 1985. "FOS Calibration Report".

Hartig, G. 1984. "UVSTOS Lamp Alignment", May 9, 1984, ST ScI ISB memo.

Hass, G. and Hunter, W.R. 1970. Applied Optics 9, 2101.

Heaney, J.B., Herzig, H. and Osantowski, J.F. 1977. Applied Optics 16, 1886.

Herzig, H. 1984. "Inspection of FOS Optics", September 7, 1984, memo to Code 400.2 GSFC.

Ott, W.R., Bridges, J.M. and Klose, J.Z. 1980. Optics Letters 5, 225.

Ott, W.R., Behringer and Gieres. 1975. Applied Optics 14, 2121.

Ott, W.R., Fieffe-Prevost and Wiese. 1973. Applied Optics 12, 1618.

Pembroke, R. 1983. Prism model in compilation of JHU test results of FOS optical components.

Pembroke, R. 1984. "Grazing Mirror Reflectance Calculations", July 25, 1984, letter to R. Harms.

FIGURE CAPTIONS

Figure 2.1 NBS Mapping of VSTOS Images. Profiles of each VSTOS lamp in both horizontal (top row) and vertical (bottom row) axes were measured in the FUV (dashed curves with open symbols at the measured points) and the NUV (solid curves with asterisks). Note the strong dependence of the profiles of the krypton and argon lamps on wavelength and the relative flatness of the diffused Pt-Cr/Ne #1 (HC #1) lamp. The profiles are normalized to the intensity at the nominal alignment of the VSTOS to the NBS monochromator, as determined by maximizing the Pt-Cr/Ne #2 (HC #2) signal. See section 2.3.2.2. of the text.

Figure 2.2 Relative Response of NBS System to VSTOS Beam. The NBS monochromator was mapped at ten wavelengths over the solid angle describing the VSTOS f/24 beam. The average response of the NBS system relative to that of the argon arc beam on axis is plotted here and used to correct the VSTOS measurements. See section 2.4.2.2 of the text.

Figure 2.3 VSTOS Krypton Lamp Calibration History. The NBS monochromator signal at two wavelengths for each of the calibration measurements, relative to that of the adopted VSTOS calibration, is plotted against the operation time accumulated since the start of the NBS activities. Also plotted (and connected by dashed lines) are the signal levels that would have been required to produce FOS QTs equal to those predicted from the component data for the H13 (λ1440) and H27 (λ2450) gratings, based on the FOS count rates measured with those gratings during the T/V-3 and August ambient APCs. The rapid degradation of the signal evident during the NBS runs did not occur during the T/V-3 measurements. See section 2.4.5 of the text.

Figure 2.4 VSTOS Argon Lamp Calibration History. See Figure 2.3 caption. The large increase in the signal from the May to August calibrations for the FUV continuum (e.g. λ1275) and its erratic behavior during the latter calibration render the lamp of little value for the QT determination at short wavelengths.

Figures 3.1-3.4 Ambient APC Results. Measurements of the FOS throughput efficiency for the G270H (H27), G400H (H40), G570H (H57), G780H (H78) and G650L (L65) gratings and the Prism, made with the ASTOS, are plotted as +'s. The predicted QTs, derived from separate determinations of the component efficiencies, are shown as dashed curves. Representative error bars are superimposed on both measured and predicted QT curves. See sections 3.2 and 4.3 of the text.

Figures 3.5-3.9 Vacuum APC Results for the Blue Side. Measurements of the FOS QTs, made with the VSTOS during T/V-3, for the G130H (H13), G190H (H19), G270H (H27) and G160L (L15) gratings and the Prism, on the blue side only, are plotted as symbols connected by solid lines, while the 'predicted' QTs are shown as dashed curves. The symbols used to denote measurements made with each of the five VSTOS lamps are: Pt-Cr/Ne#1 (+), Pt-Cr/Ne#2 (x), Argon (triangles), Krypton (diamonds), and Hydrogen (squares), as keyed in Figures 3.5 and 3.6 . Representative error bars are superimposed on both measured and 'predicted' QT curves. See sections 3.3 and 4.3 of the text.

Figures 5.1-5.4 Final QT Estimates. The best estimates of the actual FOS QTs for each of the disperser/detector combinations, derived from the APC and component measurements as analyzed in section 5, are plotted as solid curves. The predicted QTs, shown as dashed curves, are again included for

comparison. Representative error bars, indicating the bounds within which the actual QTs must reside, are superimposed on the estimated QT curves. In general, these error bars overlap those of the predicted QTs, but the measured QTs are generally about 25% lower, independent of disperser and wavelength. This may be interpreted as due to relatively minor degradation of the efficiency of each of the 4 to 6 exposed optical surfaces, with a possible contribution from a small amount of optical misalignment of the FOS components.

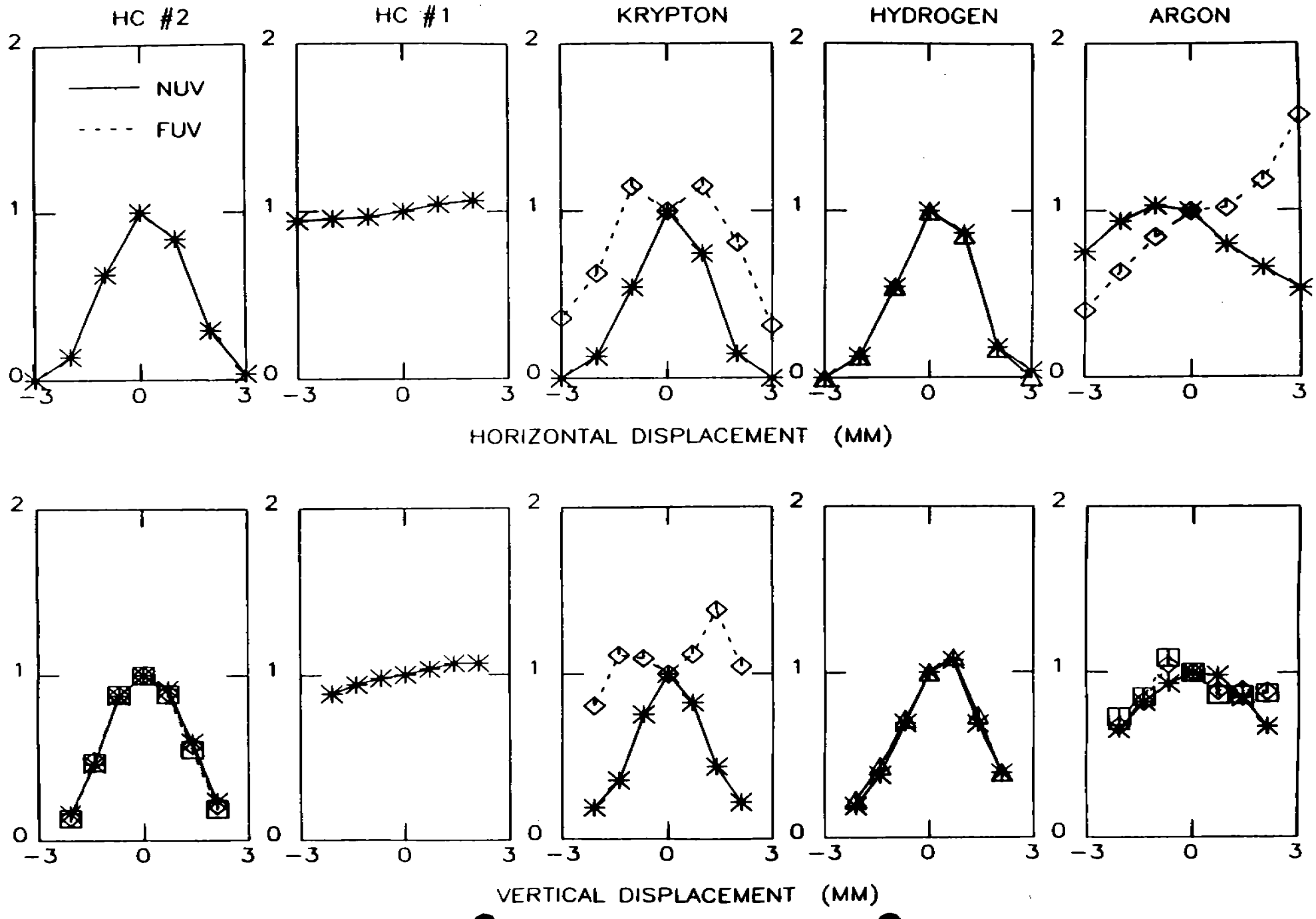

Figure 2.1 NBS Mapping of VSTOS Images

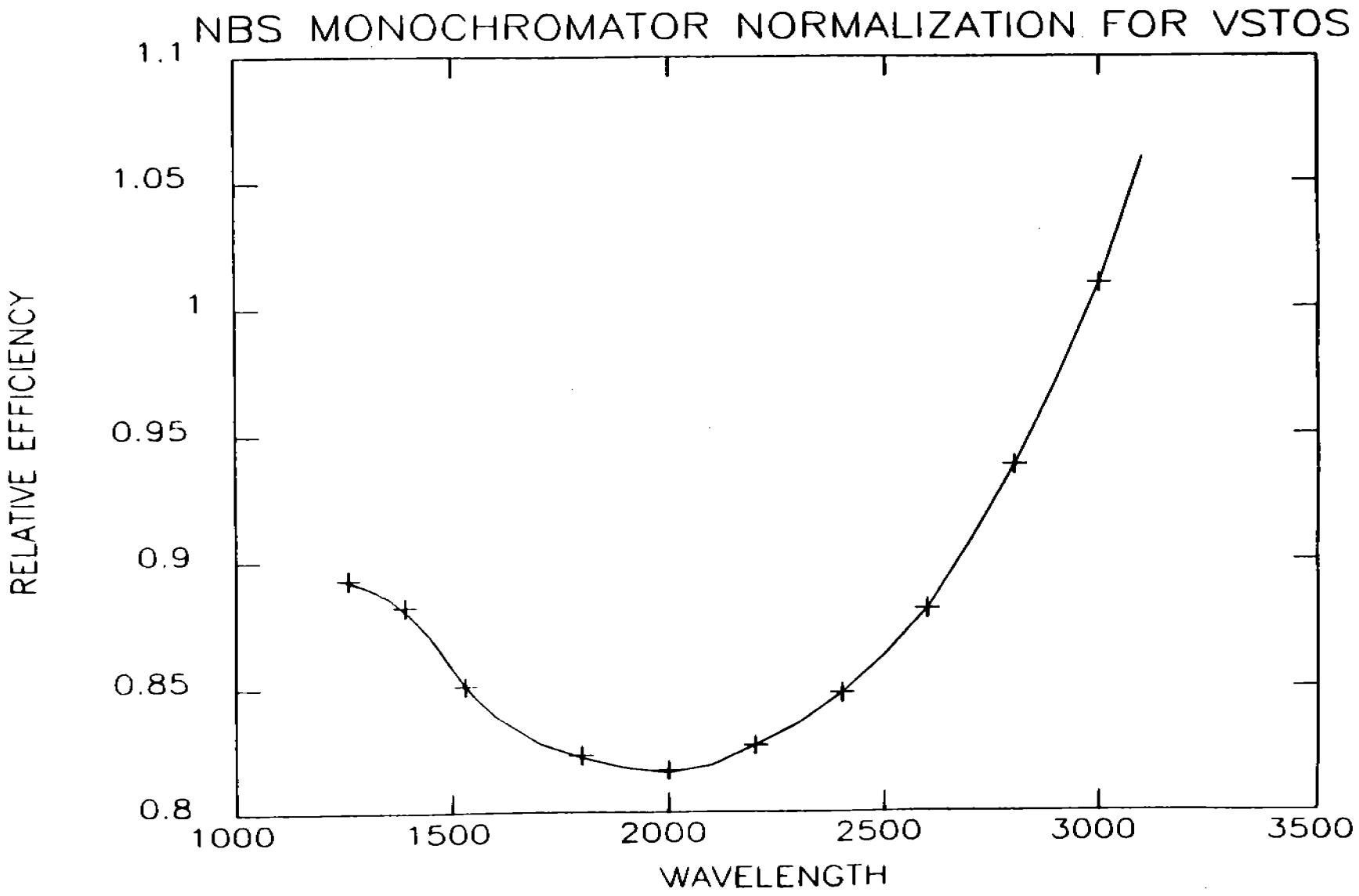

Figure 2.2 Relative Response of NBS System to VSTOS Beam

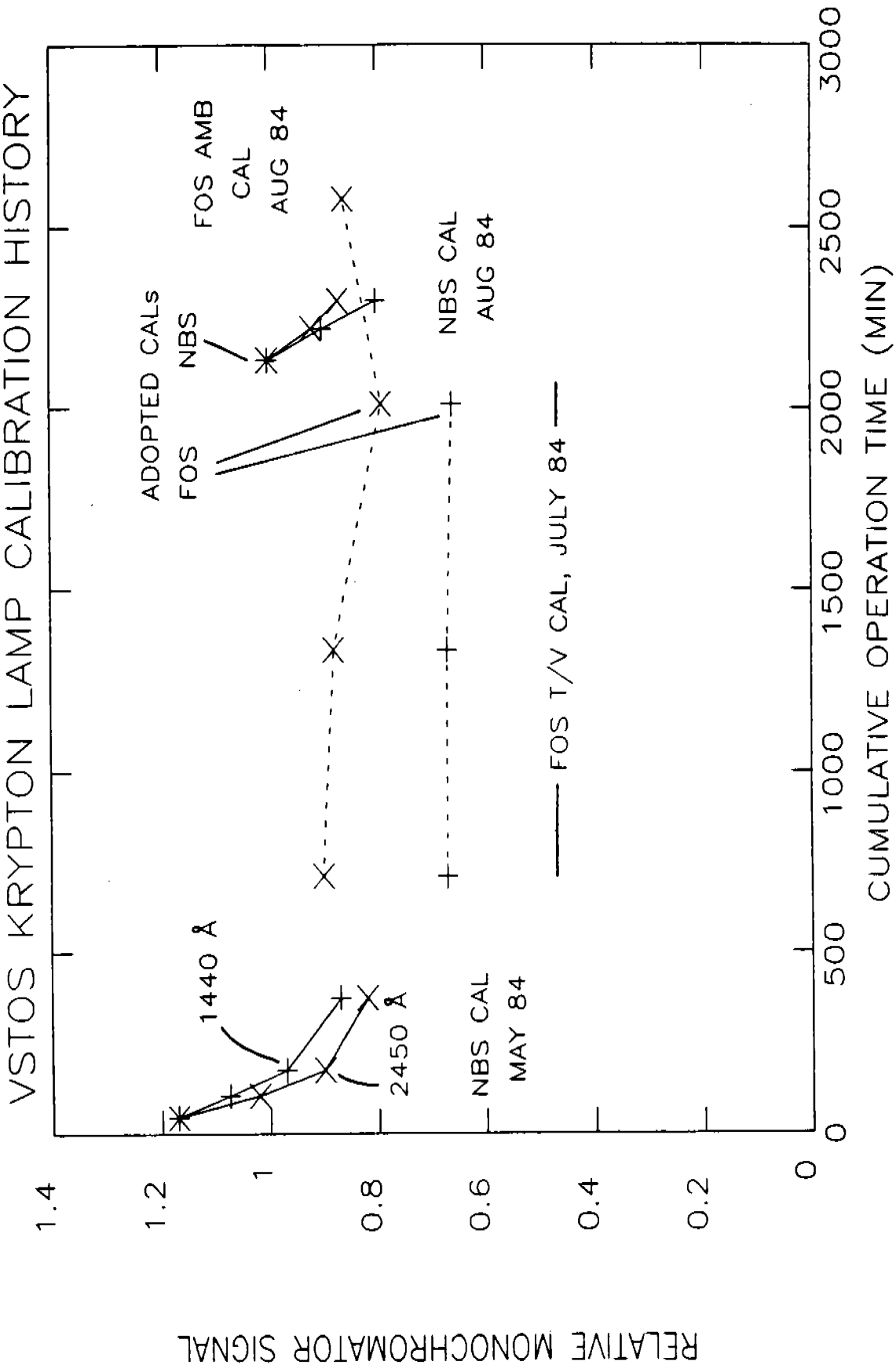

Figure 2.3 VSTOS Krypton Lamp Calibration History

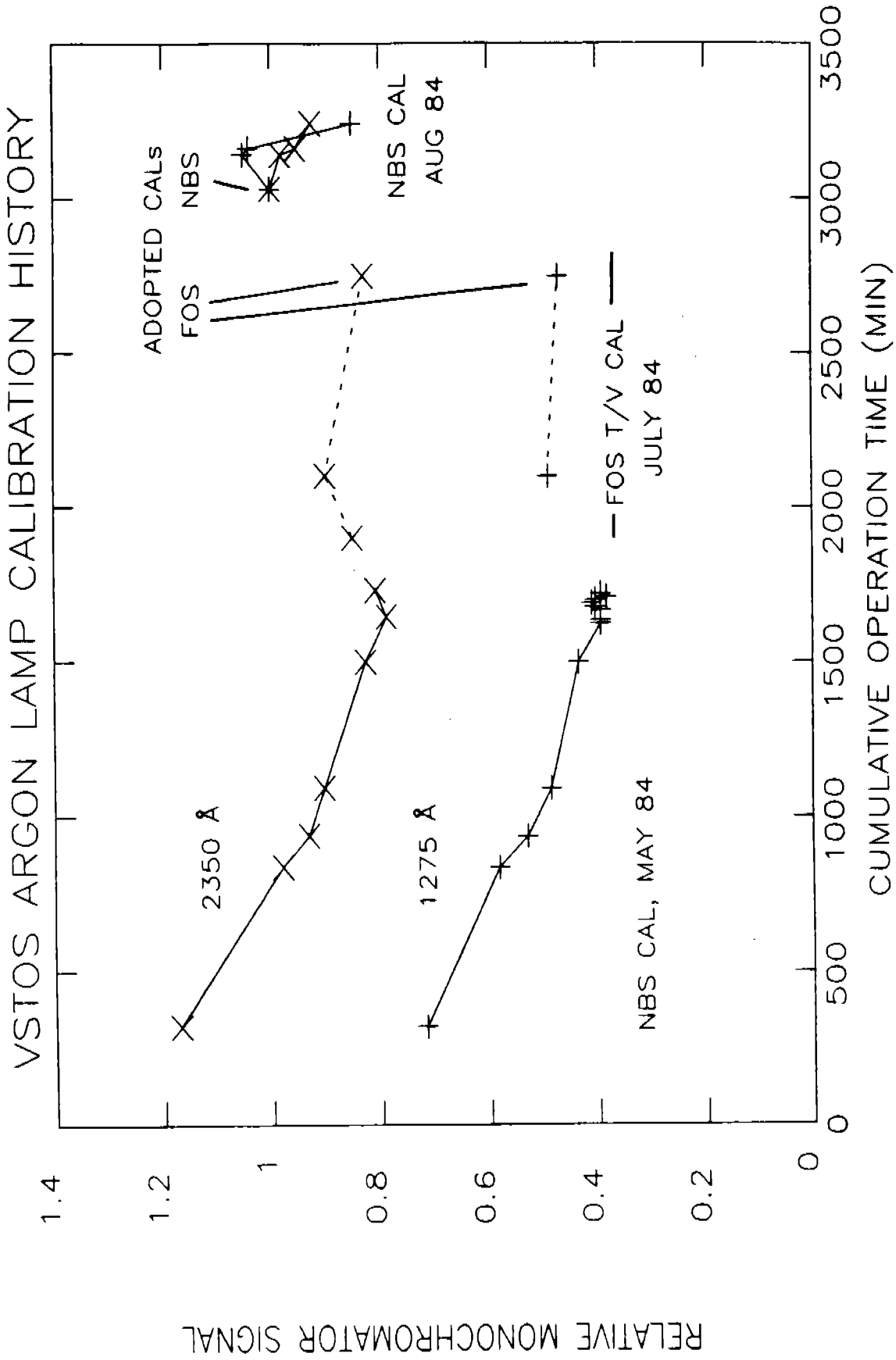

Figure 2.4 VSTOS Argon Lamp Calibration History

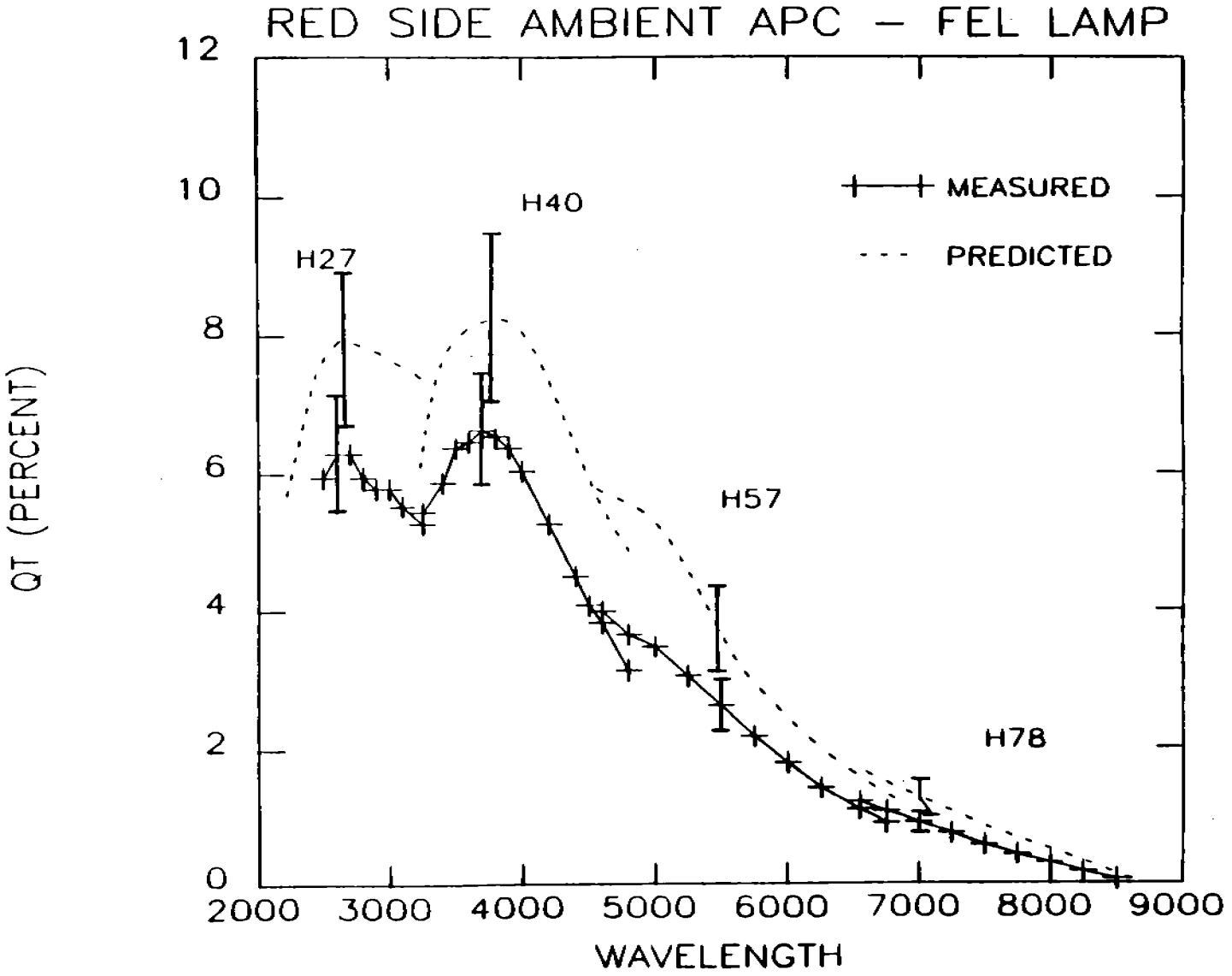

Figure 3.1 Ambient APC - Red Side High Resolution Gratings

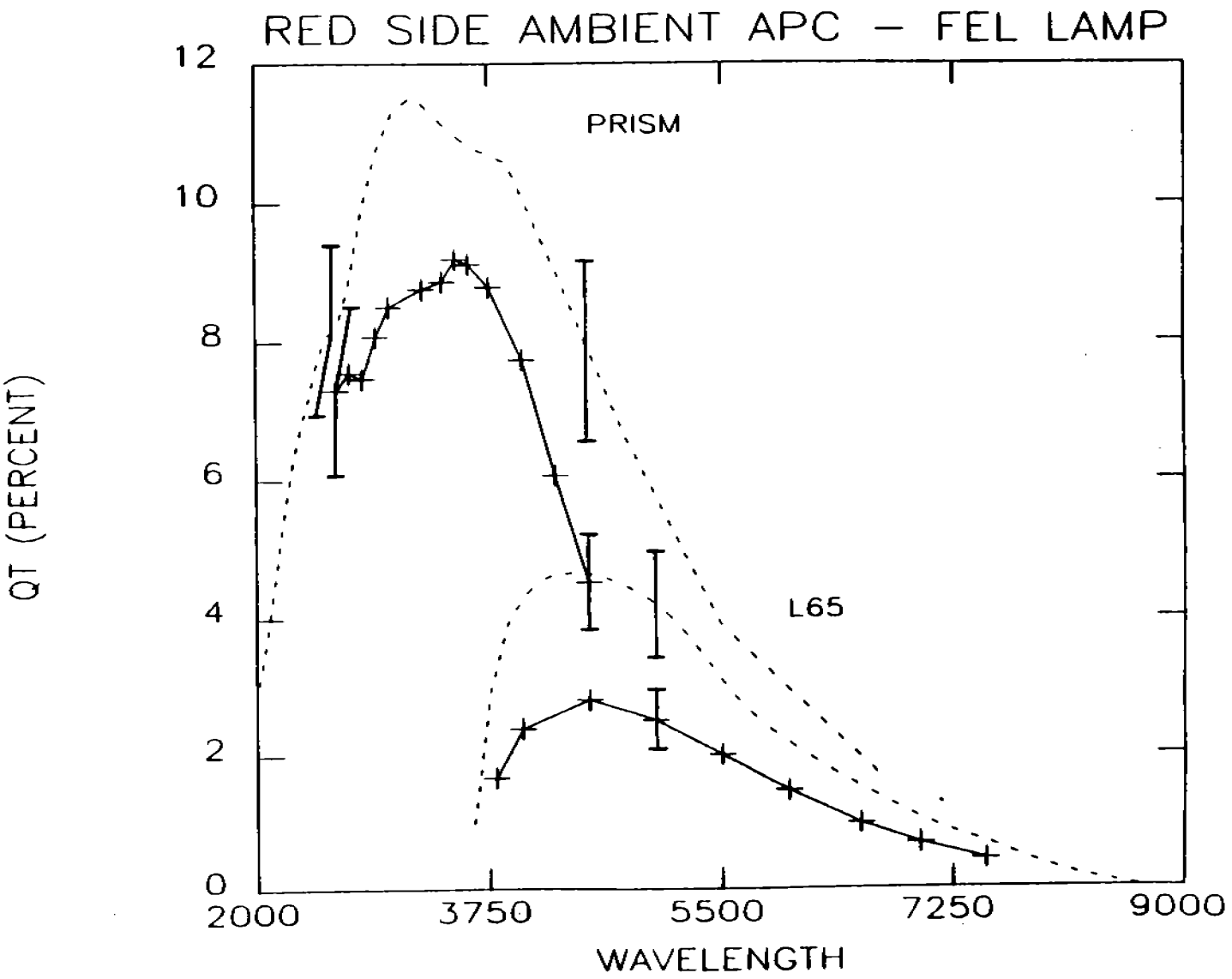

Figure 3.2 Ambient APC - Red Side Low Resolution Dispersers

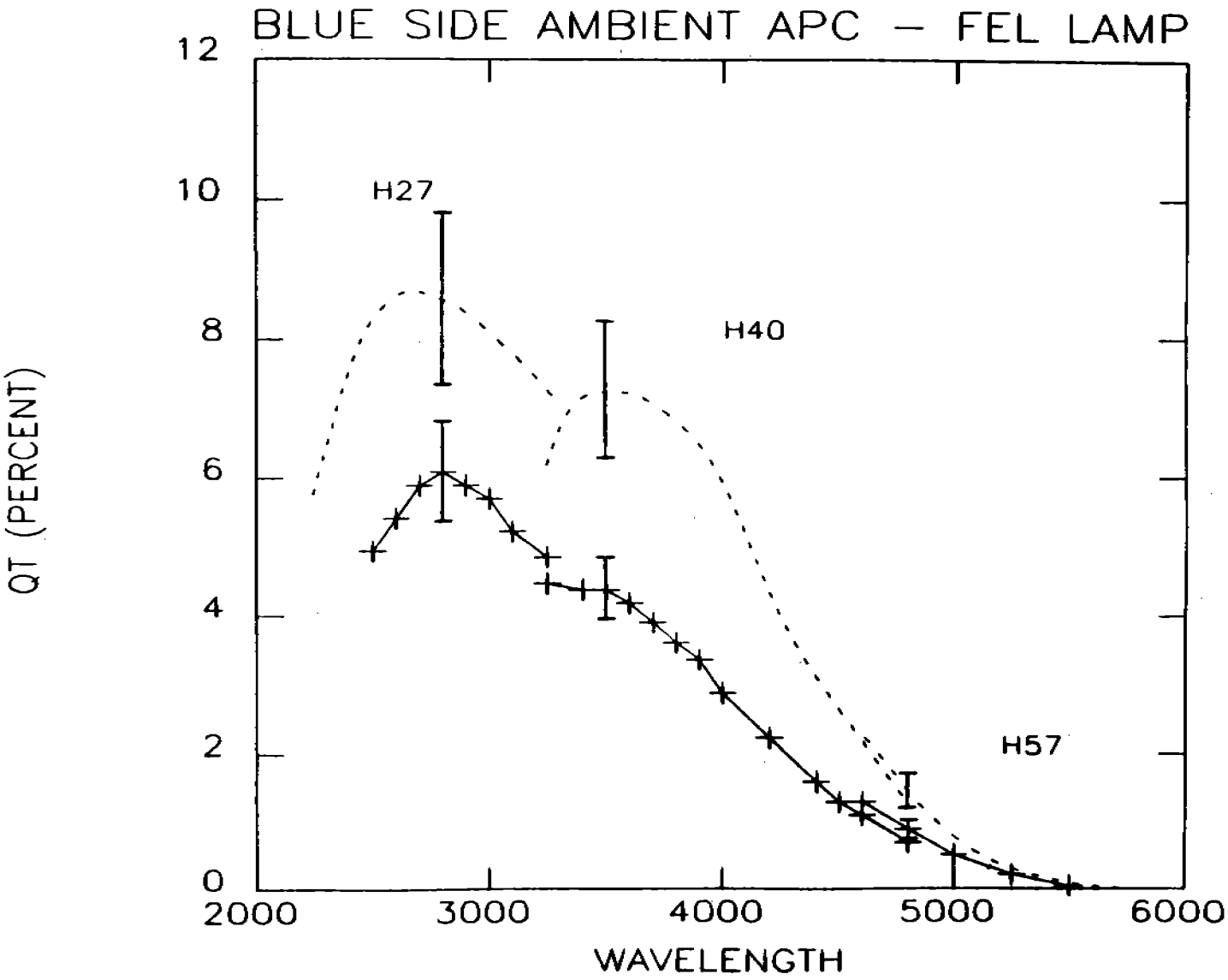

Figure 3.3 Ambient APC - Blue Side High Resolution Gratings

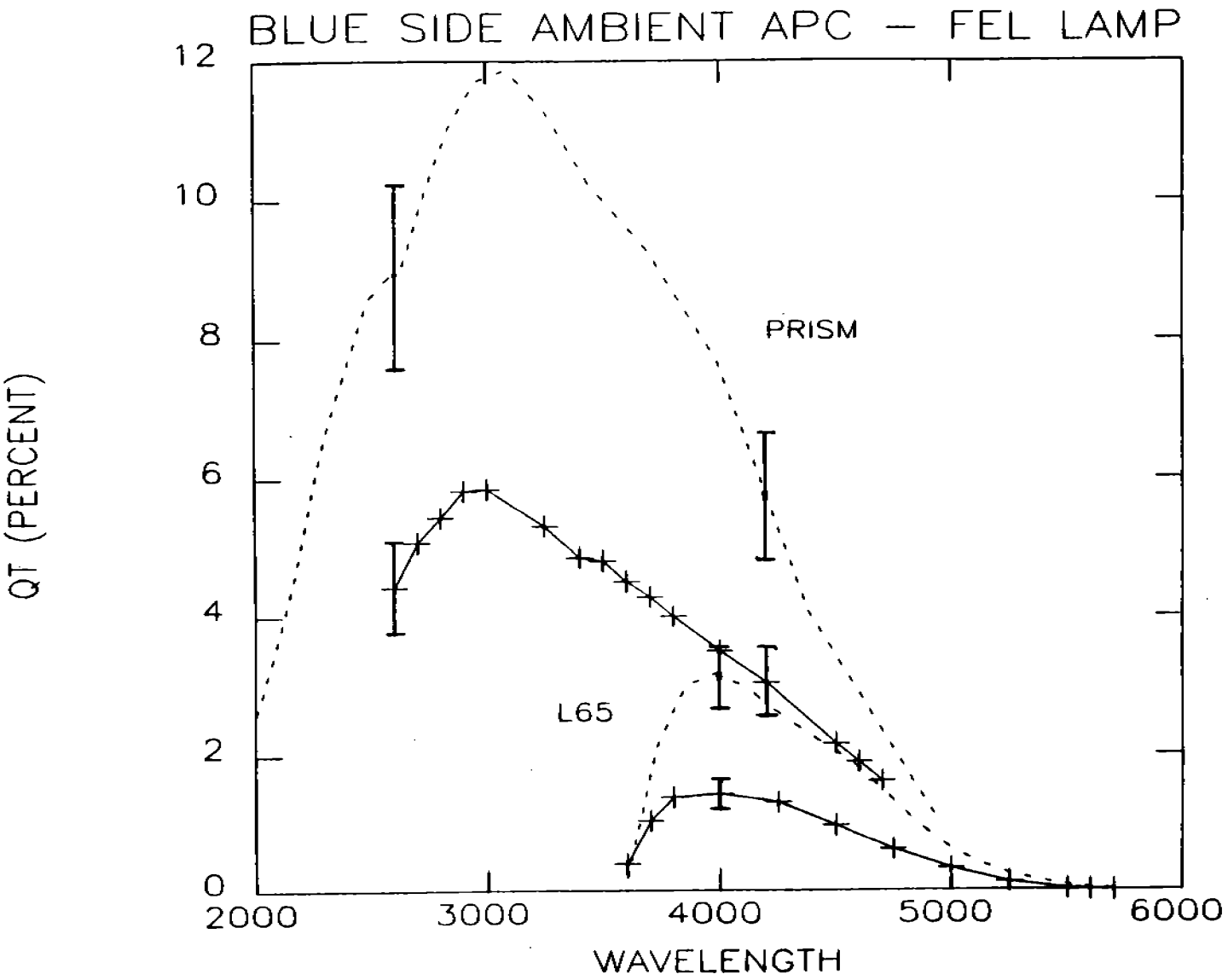

Figure 3.4 Ambient APC - Blue Side Low Resolution Dispersers

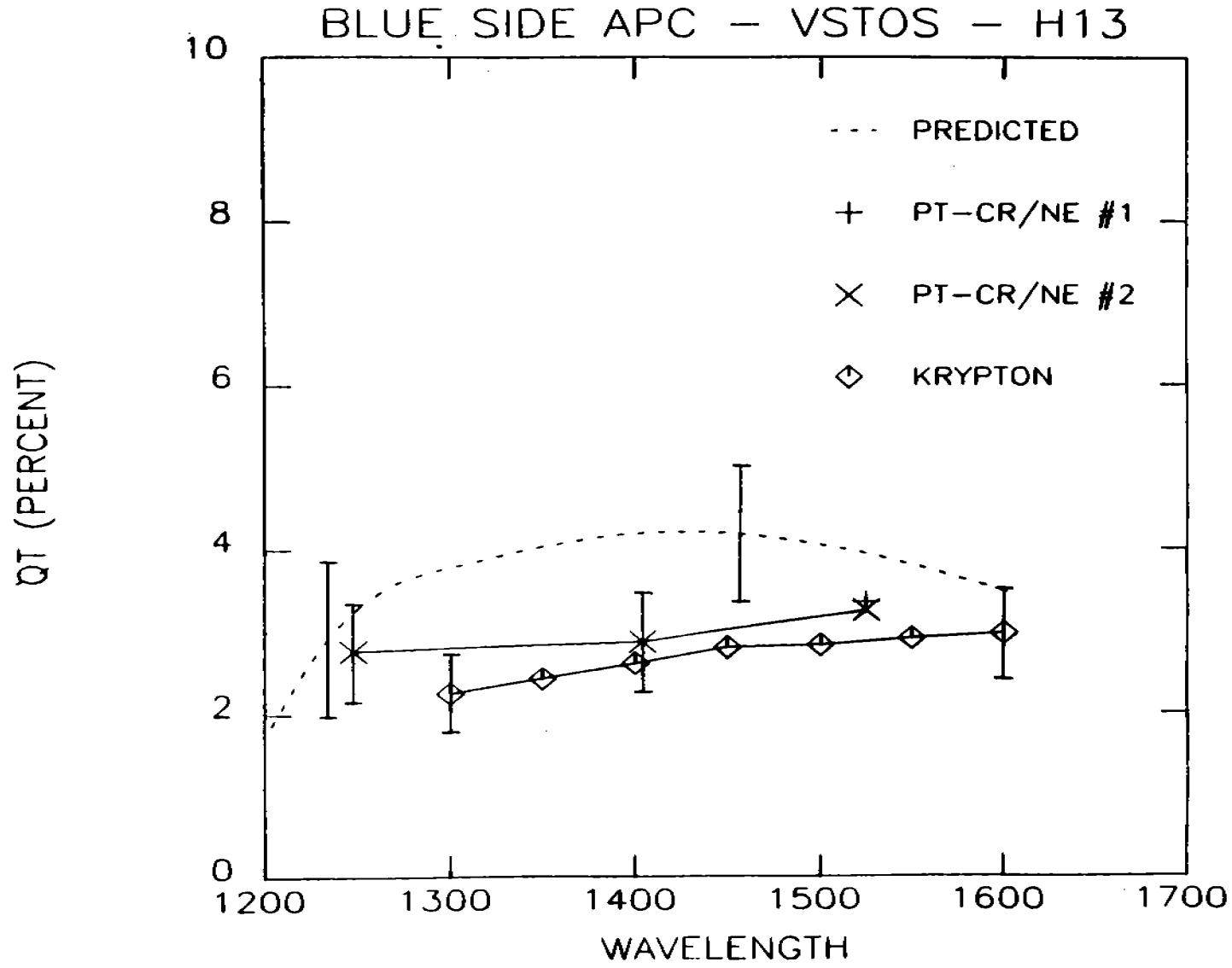

Figure 3.5 Vacuum APC - Blue Side G130H

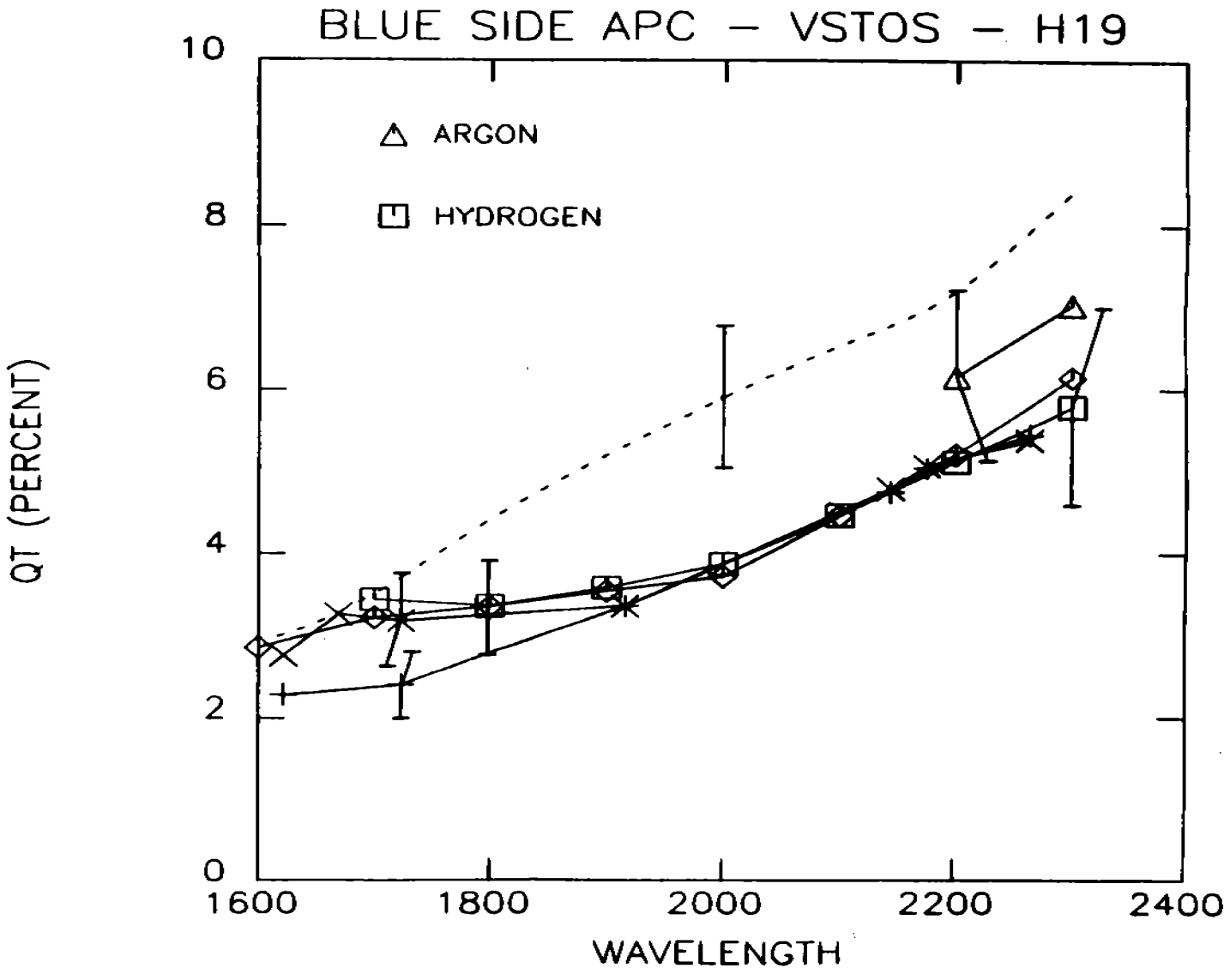

Figure 3.6 Vacuum APC - Blue Side G190H

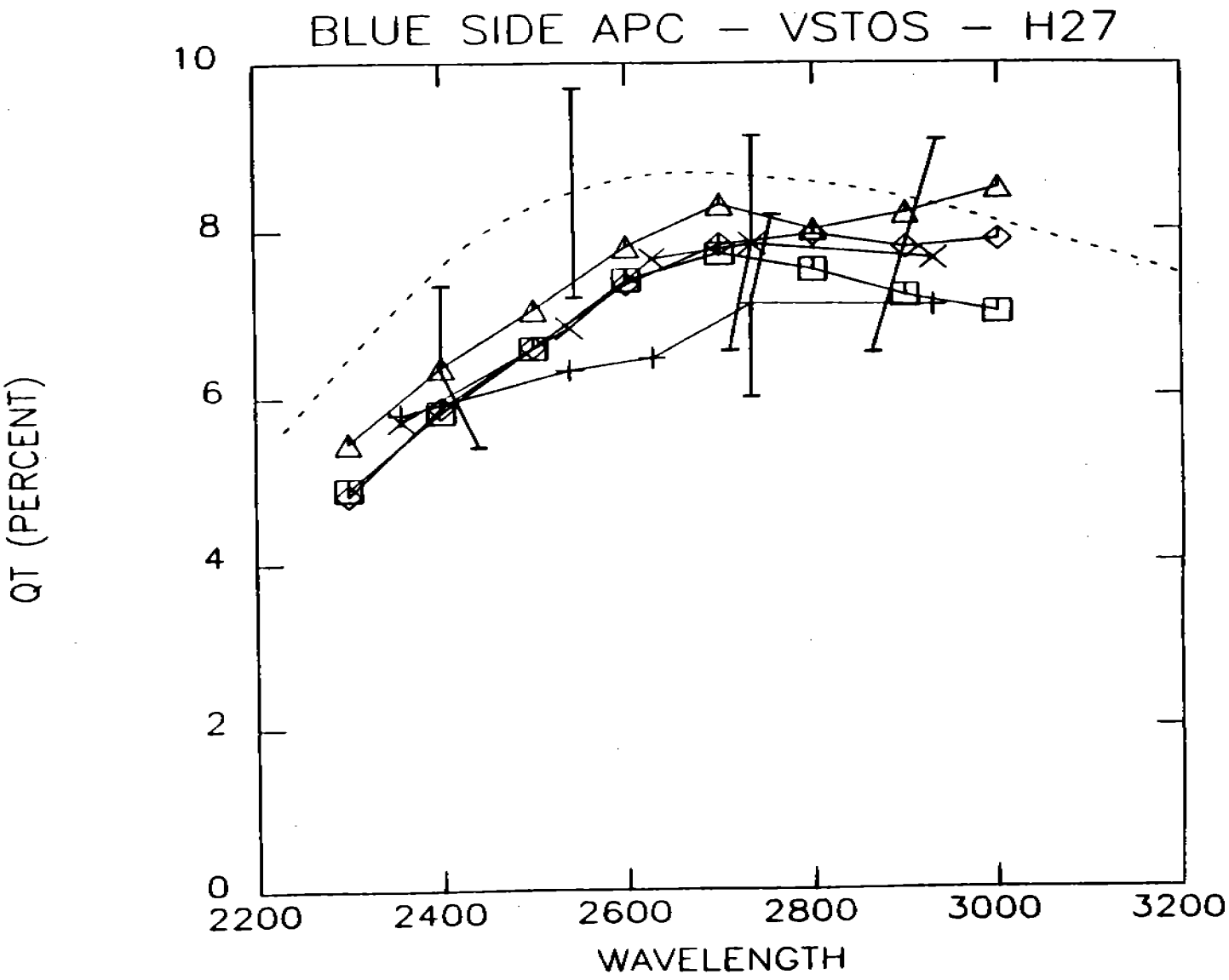

Figure 3.7 Vacuum APC - Blue Side G270H

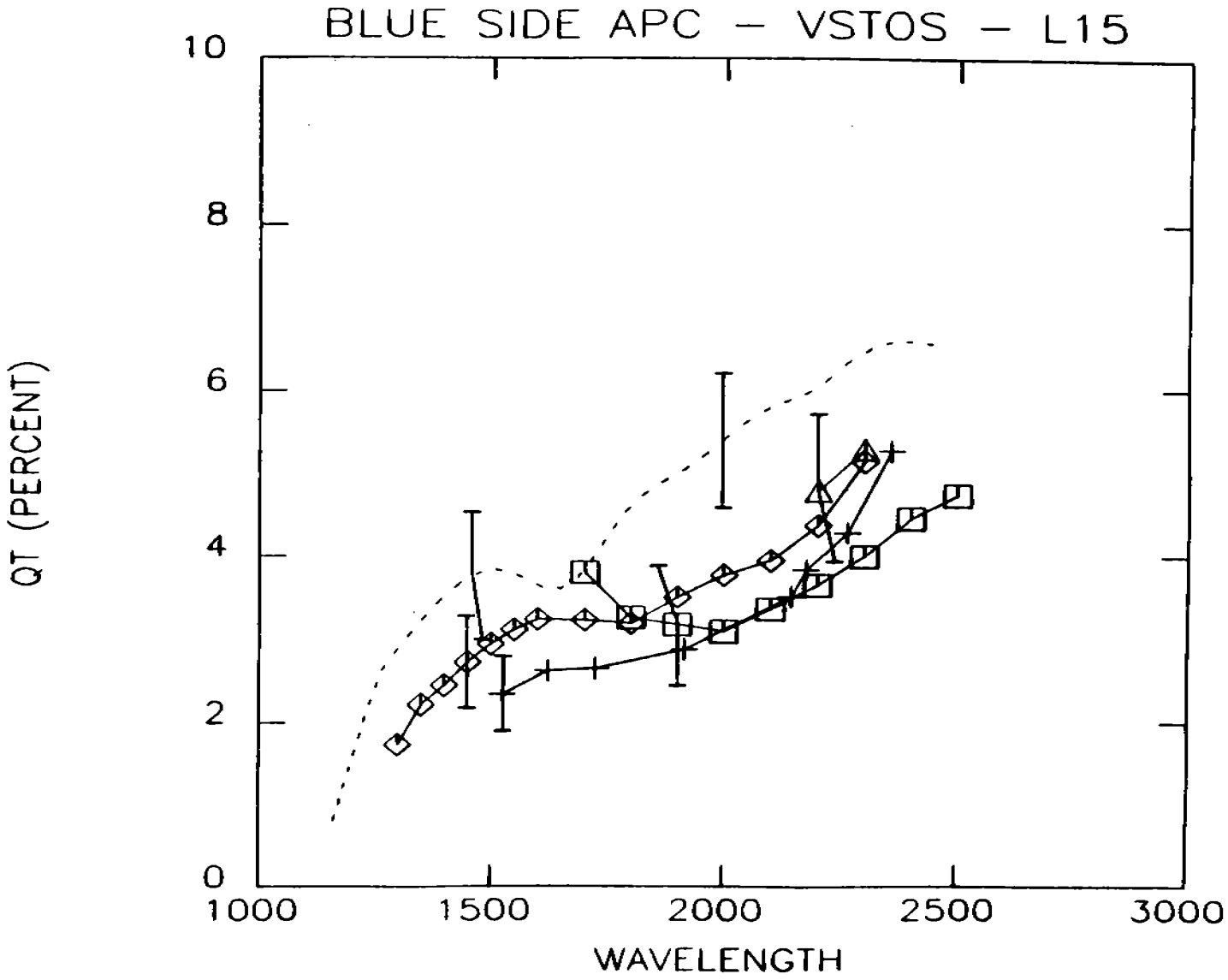

Figure 3.8 Vacuum APC - Blue Side G160L

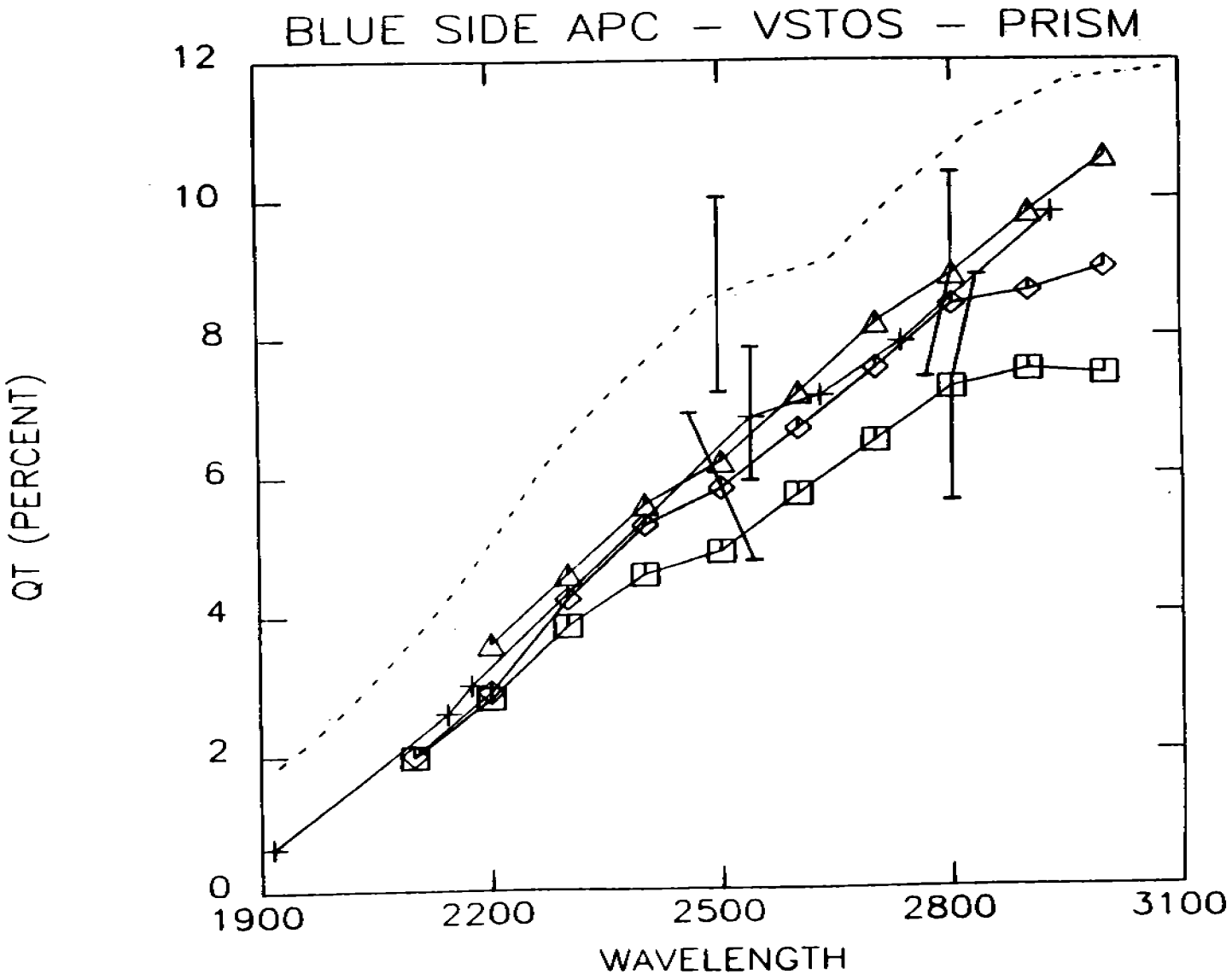

Figure 3.9 Vacuum APC - Blue Side Prism

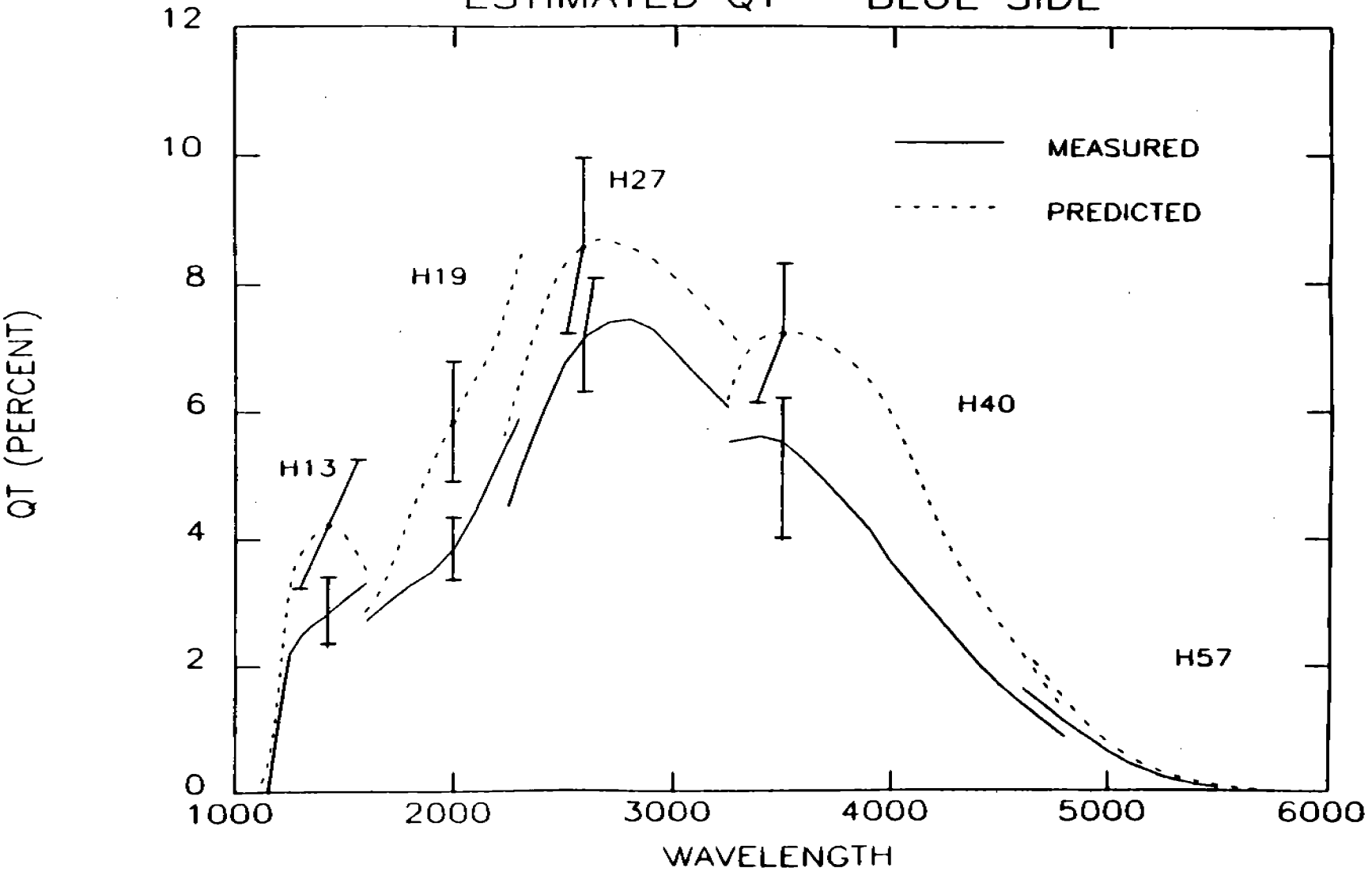

Figure 5.1 Final QT Estimates - Blue Side High Resolution Gratings

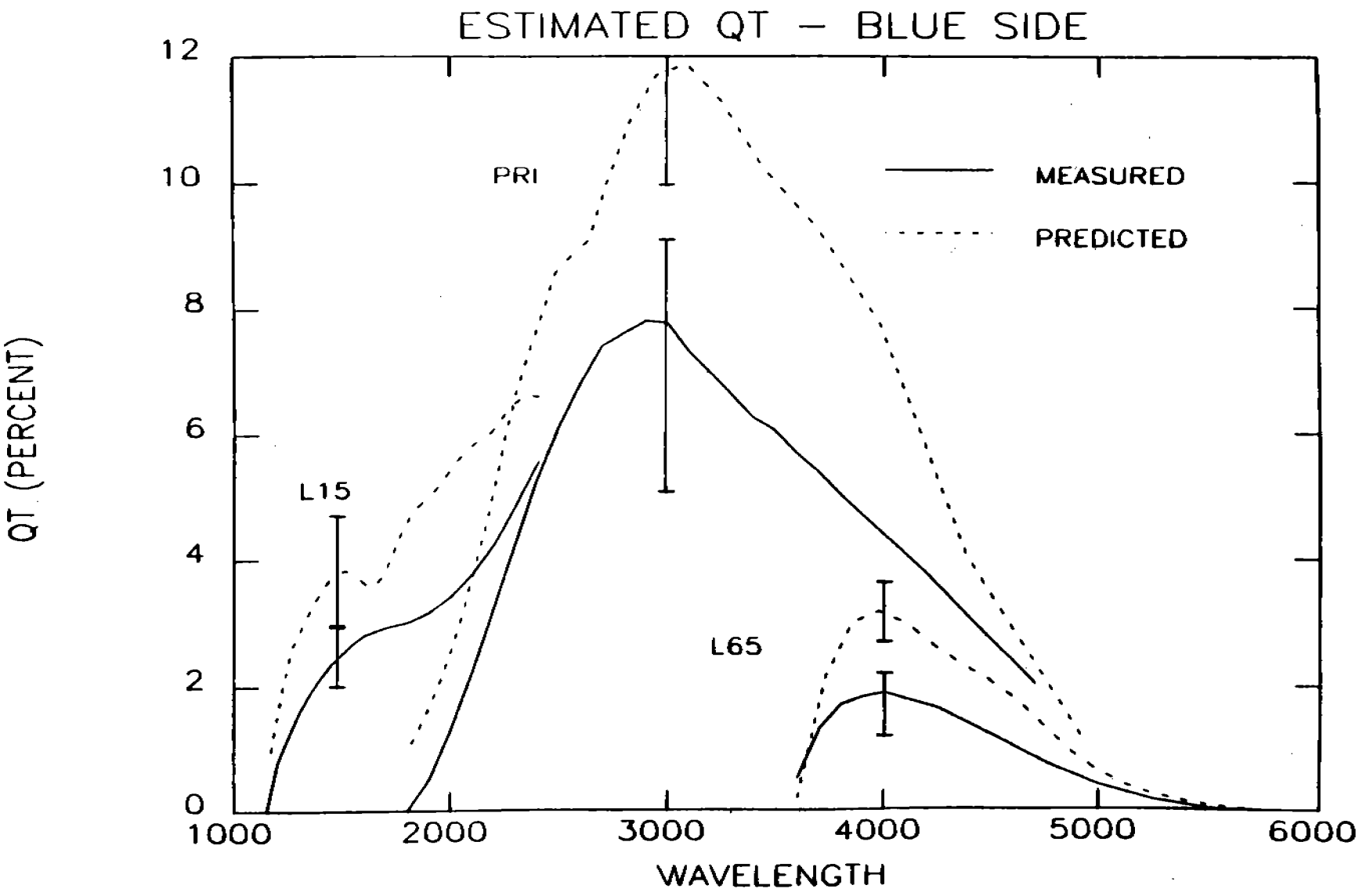

Figure 5.2 Final QT Estimates - Blue Side Low Resolution Dispersers

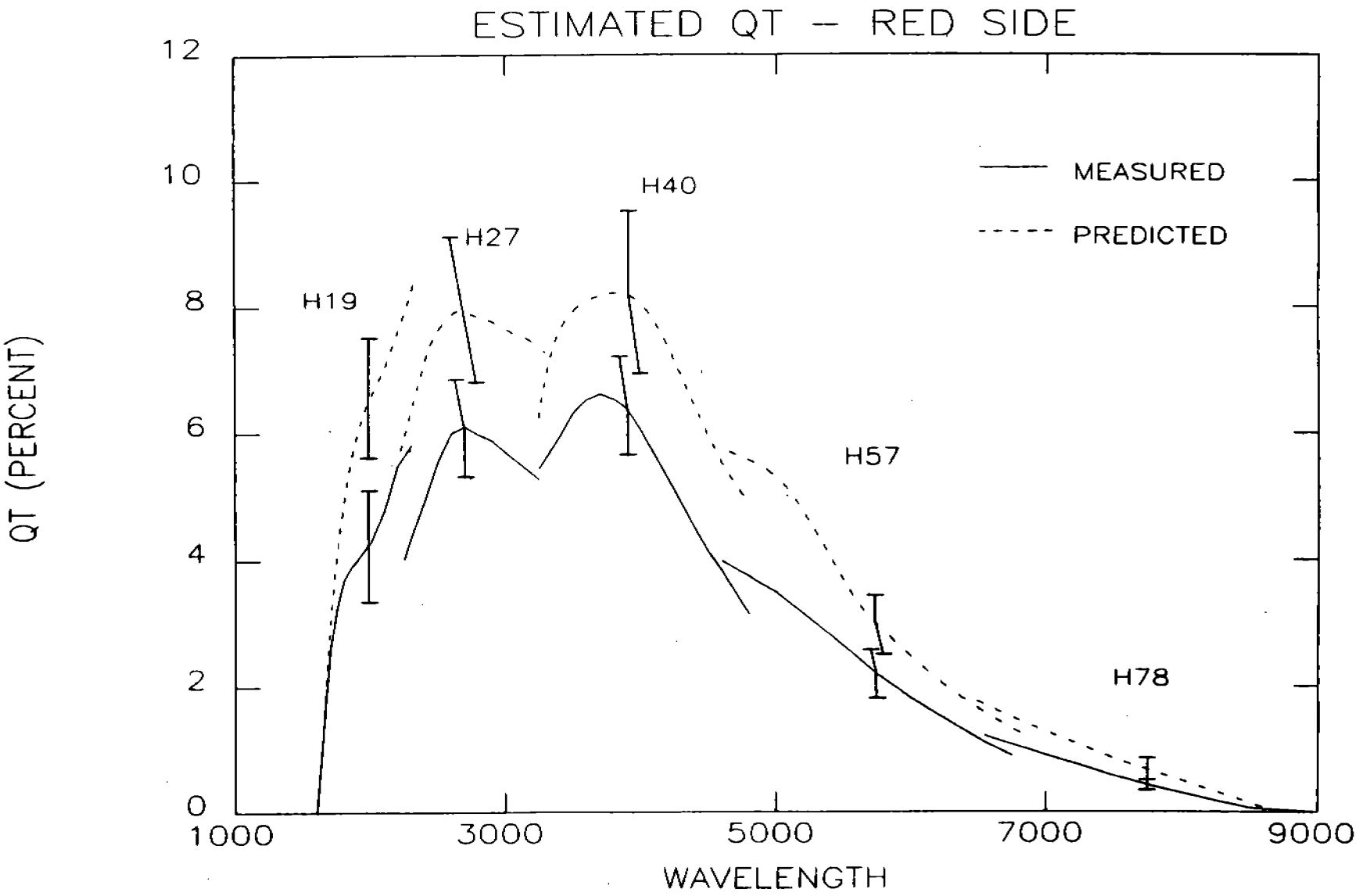

Figure 5.3 Final QT Estimates - Red Side High Resolution Gratings

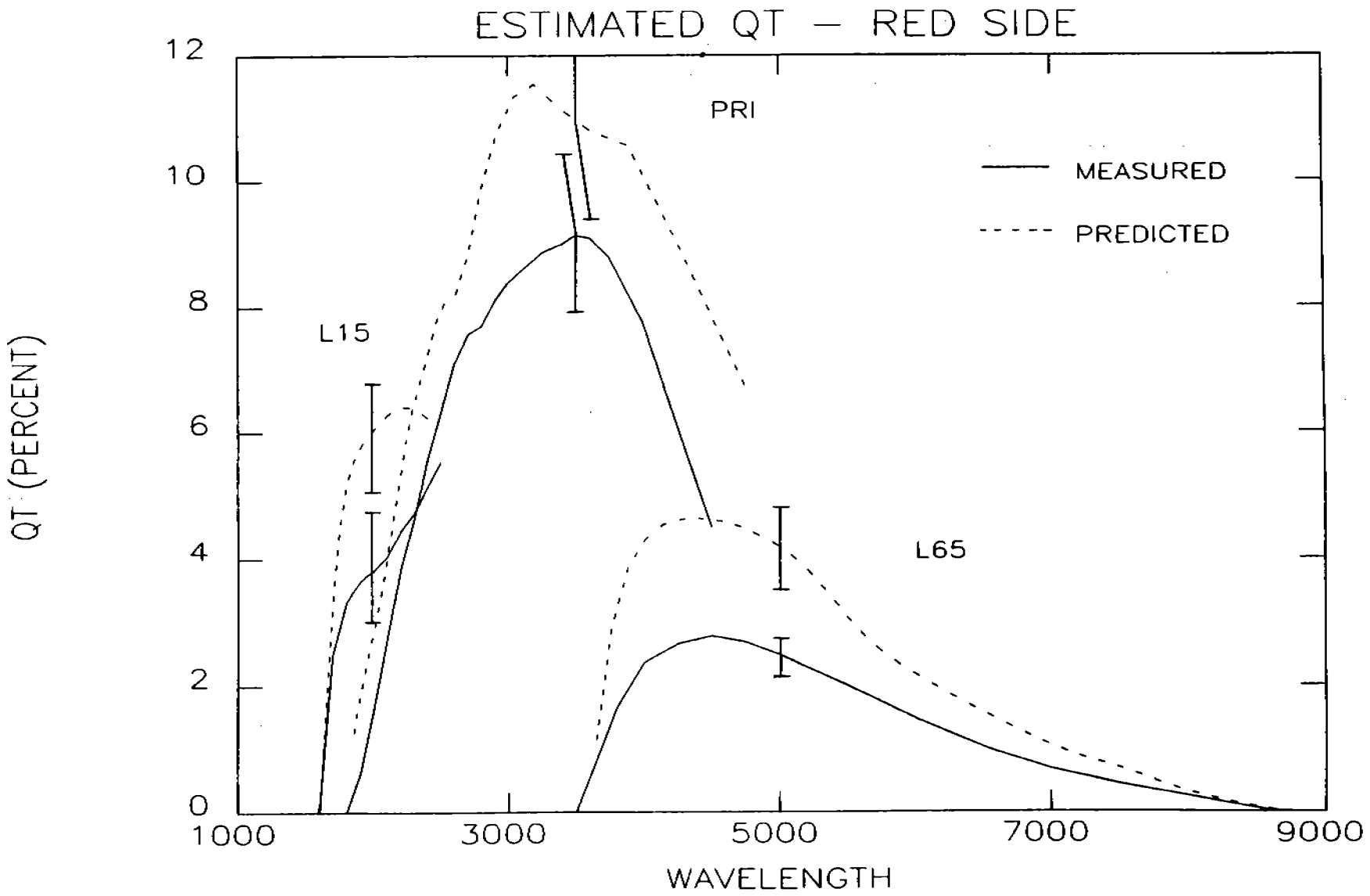

Figure 5.4 Final QT Estimates - Red Side Low Resolution Dispersers

APPENDIX A

TABLES OF ESTIMATED FOS QT

H13 BLUE	
WAV.	QT
1160.	0.0025
1180.	0.0065
1200.	0.0113
1220.	0.0168
1240.	0.0204
1260.	0.0224
1280.	0.0239
1300.	0.0250
1320.	0.0258
1340.	0.0264
1360.	0.0268
1380.	0.0273
1400.	0.0278
1420.	0.0283
1440.	0.0289
1460.	0.0295
1480.	0.0301
1500.	0.0307
1520.	0.0312
1540.	0.0317
1560.	0.0323
1580.	0.0328
1600.	0.0333

H19 BLUE	
WAV.	QT
1580.	0.0268
1600.	0.0274
1620.	0.0280
1640.	0.0286
1660.	0.0292
1680.	0.0297
1700.	0.0303
1720.	0.0309
1740.	0.0314
1760.	0.0319
1780.	0.0324
1800.	0.0329
1820.	0.0333
1840.	0.0337
1860.	0.0340
1880.	0.0344
1900.	0.0349
1920.	0.0354
1940.	0.0361
1960.	0.0368
1980.	0.0376
2000.	0.0385
2020.	0.0395
2040.	0.0406
2060.	0.0418
2080.	0.0430
2100.	0.0444
2120.	0.0459
2140.	0.0474
2160.	0.0489
2180.	0.0505
2200.	0.0520
2220.	0.0535
2240.	0.0549
2260.	0.0563
2280.	0.0577
2300.	0.0591
2320.	0.0605

H27 BLUE	
WAV.	QT
2250.	0.0452
2300.	0.0506
2350.	0.0552
2400.	0.0595
2450.	0.0638
2500.	0.0675
2550.	0.0702
2600.	0.0720
2650.	0.0732
2700.	0.0740
2750.	0.0744
2800.	0.0745
2850.	0.0740
2900.	0.0730
2950.	0.0714
3000.	0.0695
3050.	0.0676
3100.	0.0658
3150.	0.0640
3200.	0.0623
3250.	0.0607
3300.	0.0591

H40 BLUE	
WAV.	QT
3250.	0.0552
3300.	0.0558
3350.	0.0561
3400.	0.0561
3450.	0.0559
3500.	0.0552
3550.	0.0540
3600.	0.0524
3650.	0.0506
3700.	0.0488
3750.	0.0469
3800.	0.0451
3850.	0.0434
3900.	0.0414
3950.	0.0389
4000.	0.0362
4050.	0.0339
4100.	0.0319
4150.	0.0301
4200.	0.0282
4250.	0.0262
4300.	0.0242
4350.	0.0221
4400.	0.0202
4450.	0.0184
4500.	0.0168
4550.	0.0153
4600.	0.0139
4650.	0.0125
4700.	0.0112
4750.	0.0099
4800.	0.008

H57 BLUE

WAV.	QT
4600.	0.0164
4650.	0.0150
4700.	0.0137
4750.	0.0124
4800.	0.0111
4850.	0.0098
4900.	0.0086
4950.	0.0074
5000.	0.0063
5050.	0.0053
5100.	0.0044
5150.	0.0036
5200.	0.0029
5250.	0.0023
5300.	0.0018
5350.	0.0013
5400.	0.0010
5450.	0.0008
5500.	0.0006
5550.	0.0005
5600.	0.0003
5650.	0.0002
5700.	0.0001
5750.	0.0001
5800.	0.0000
5850.	0.0000
5900.	0.0000
5950.	0.0000
6000.	0.0000

L15 BLUE

WAV.	QT
1150.	0.0006
1200.	0.0077
1250.	0.0125
1300.	0.0159
1350.	0.0190
1400.	0.0216
1450.	0.0238
1500.	0.0254
1550.	0.0270
1600.	0.0282
1650.	0.0289
1700.	0.0294
1750.	0.0298
1800.	0.0302
1850.	0.0308
1900.	0.0317
1950.	0.0328
2000.	0.0341
2050.	0.0357
2100.	0.0375
2150.	0.0397
2200.	0.0422
2250.	0.0451
2300.	0.0483
2350.	0.0517
2400.	0.0550
2450.	0.0577
2500.	0.0600

L65 BLUE

WAV.	QT
3500.	0.0000
3600.	0.0051
3700.	0.0131
3800.	0.0170
3900.	0.0183
4000.	0.0188
4100.	0.0181
4200.	0.0170
4300.	0.0157
4400.	0.0140
4500.	0.0121
4600.	0.0102
4700.	0.0085
4800.	0.0068
4900.	0.0053
5000.	0.0040
5100.	0.0029
5200.	0.0020
5300.	0.0013
5400.	0.0007
5500.	0.0003
5600.	0.0001
5700.	0.0001
5800.	0.0001
5900.	0.0001
6000.	0.0000

PRI BLUE

WAV.	QT
1800.	0.0000
1900.	0.0050
2000.	0.0131
2100.	0.0224
2200.	0.0324
2300.	0.0424
2400.	0.0526
2500.	0.0610
2600.	0.0680
2700.	0.0740
2800.	0.0760
2900.	0.0780
3000.	0.0777
3100.	0.0731
3200.	0.0697
3300.	0.0662
3400.	0.0626
3500.	0.0605
3600.	0.0569
3700.	0.0539
3800.	0.0503
3900.	0.0470
4000.	0.0440
4100.	0.0409
4200.	0.0377
4300.	0.0342
4400.	0.0306
4500.	0.0272

H19 RED

WAV.	QT
1600.	0.0000
1620.	0.0053
1640.	0.0107
1660.	0.0162
1680.	0.0217
1700.	0.0264
1720.	0.0297
1740.	0.0319
1760.	0.0338
1780.	0.0355
1800.	0.0369
1820.	0.0379
1840.	0.0385
1860.	0.0391
1880.	0.0396
1900.	0.0401
1920.	0.0406
1940.	0.0411
1960.	0.0416
1980.	0.0422
2000.	0.0429
2020.	0.0437
2040.	0.0445
2060.	0.0455
2080.	0.0466
2100.	0.0479
2120.	0.0493
2140.	0.0508
2160.	0.0523
2180.	0.0538
2200.	0.0550
2220.	0.0560
2240.	0.0568
2260.	0.0574
2280.	0.0578
2300.	0.0581

H27 RED

WAV.	QT
2250.	0.0403
2300.	0.0437
2350.	0.0467
2400.	0.0495
2450.	0.0525
2500.	0.0555
2550.	0.0581
2600.	0.0600
2650.	0.0609
2700.	0.0610
2750.	0.0605
2800.	0.0598
2850.	0.0593
2900.	0.0588
2950.	0.0580
3000.	0.0570
3050.	0.0561
3100.	0.0553
3150.	0.0545
3200.	0.0536
3250.	0.0527
3300.	0.0518

H40 RED

WAV.	QT
3250.	0.0544
3300.	0.0560
3350.	0.0577
3400.	0.0595
3450.	0.0615
3500.	0.0633
3550.	0.0645
3600.	0.0654
3650.	0.0660
3700.	0.0663
3750.	0.0660
3800.	0.0654
3850.	0.0648
3900.	0.0638
3950.	0.0623
4000.	0.0604
4050.	0.0585
4100.	0.0565
4150.	0.0546
4200.	0.0527
4250.	0.0508
4300.	0.0489
4350.	0.0470
4400.	0.0450
4450.	0.0430
4500.	0.0412
4550.	0.0397
4600.	0.0383
4650.	0.0368
4700.	0.0351
4750.	0.0333
4800.	0.0314

H57 RED

WAV.	QT
4600.	0.0399
4650.	0.0393
4700.	0.0386
4750.	0.0380
4800.	0.0374
4850.	0.0368
4900.	0.0362
4950.	0.0356
5000.	0.0349
5050.	0.0341
5100.	0.0333
5150.	0.0324
5200.	0.0315
5250.	0.0306
5300.	0.0297
5350.	0.0289
5400.	0.0281
5450.	0.0273
5500.	0.0264
5550.	0.0255
5600.	0.0246
5650.	0.0236
5700.	0.0227
5750.	0.0218
5800.	0.0210
5850.	0.0202
5900.	0.0194
5950.	0.0187
6000.	0.0180
6050.	0.0173
6100.	0.0167
6150.	0.0161
6200.	0.0154
6250.	0.0148
6300.	0.0142
6350.	0.0135
6400.	0.0129
6450.	0.0122
6500.	0.0116
6550.	0.0111
6600.	0.0105
6650.	0.0100
6700.	0.0095
6750.	0.0090
6800.	0.0085
6850.	0.0081

H78 RED

WAV.	QT
6300.	0.0139
6400.	0.0132
6500.	0.0125
6600.	0.0118
6700.	0.0111
6800.	0.0105
6900.	0.0098
7000.	0.0091
7100.	0.0085
7200.	0.0078
7300.	0.0072
7400.	0.0065
7500.	0.0058
7600.	0.0052
7700.	0.0046
7800.	0.0040
7900.	0.0036
8000.	0.0031
8100.	0.0026
8200.	0.0021
8300.	0.0015
8400.	0.0011
8500.	0.0007
8600.	0.0004
8700.	0.0002
8800.	0.0001
8900.	0.0000
9000.	0.0000

L15 RED

WAV.	QT
1600.	0.0000
1650.	0.0139
1700.	0.0252
1750.	0.0302
1800.	0.0334
1850.	0.0354
1900.	0.0366
1950.	0.0375
2000.	0.0382
2050.	0.0391
2100.	0.0404
2150.	0.0424
2200.	0.0444
2250.	0.0458
2300.	0.0473
2350.	0.0494
2400.	0.0516
2450.	0.0536
2500.	0.0554

L65 RED

WAV.	QT
3500.	0.0000
3600.	0.0063
3700.	0.0119
3800.	0.0167
3900.	0.0208
4000.	0.0238
4100.	0.0255
4200.	0.0265
4300.	0.0271
4400.	0.0277
4500.	0.0280
4600.	0.0278
4700.	0.0273
4800.	0.0266
4900.	0.0259
5000.	0.0250
5100.	0.0241
5200.	0.0231
5300.	0.0221
5400.	0.0211
5500.	0.0200
5600.	0.0189
5700.	0.0178
5800.	0.0168
5900.	0.0157
6000.	0.0147
6100.	0.0137
6200.	0.0128
6300.	0.0119
6400.	0.0110
6500.	0.0102
6600.	0.0094
6700.	0.0086
6800.	0.0079
6900.	0.0073
7000.	0.0067
7100.	0.0062
7200.	0.0057
7300.	0.0052
7400.	0.0047
7500.	0.0043
7600.	0.0039
7700.	0.0034
7800.	0.0030
7900.	0.0025
8000.	0.0021
8100.	0.0017
8200.	0.0013
8300.	0.0010
8400.	0.0007
8500.	0.0004
8600.	0.0002
8700.	0.0001
8800.	0.0000
8900.	0.0000

PRI RED

WAV.	QT
1800.	0.0000
1900.	0.0062
2000.	0.0164
2100.	0.0276
2200.	0.0385
2300.	0.0463
2400.	0.0559
2500.	0.0632
2600.	0.0711
2700.	0.0756
2800.	0.0770
2900.	0.0810
3000.	0.0840
3100.	0.0862
3200.	0.0879
3300.	0.0891
3400.	0.0901
3500.	0.0914
3600.	0.0910
3700.	0.0891
3800.	0.0862
3900.	0.0823
4000.	0.0773
4100.	0.0709
4200.	0.0639
4300.	0.0572
4400.	0.0510
4500.	0.0450